이학박사 학위논문

Aberrant neural activities and dynamics of functional connectivity patterns in cognitive frailty using FDG PET and resting state fMRI

인지 노쇠에서 FDG PET 과 휴지상태 fMRI 를 이용한 뇌 신경 활동과 기능적 연결성 패턴의 동적 변화 연구

2019 년 8 월

서울대학교 대학원

의과학과 전공

신 성 아

Aberrant neural activities and dynamics of functional connectivity patterns in cognitive frailty using FDG PET and resting state fMRI

지도 교수 이 재 성

이 논문을 이학박사 학위논문으로 제출함
2019 년 4 월

서울대학교 대학원
의과학과 전공
신 성 아

신성아의 이학박사 학위논문을 인준함
2019 년 7 월

위 원 장 정 천 기 (인)
부위원장 이 재 성 (인)
위 원 강 건 욱 (인)
위 원 이 인 아 (인)
위 원 김 유 경 (인)

Aberrant neural activities and dynamics of functional connectivity patterns in cognitive frailty using FDG PET and resting state fMRI

Seong A Shin

A Thesis Submitted in Partial Fulfillment of the Requirements for the Degree of Doctor of Philosophy (Ph.D.) in Science (Biomedical Sciences major) at Seoul National University

July 2019

Approved by thesis committee:

Chairman _____(Seal)

Vice Chair _____(Seal)

Member _____(Seal)

Member _____(Seal)

Member _____(Seal)

Abstract

Aberrant neural activities and dynamics of functional connectivity patterns in cognitive frailty using FDG PET and resting state fMRI

Seong A Shin

Department of Biomedical Sciences

The Graduate School

Seoul National University

Cognitive frailty is a recently defined clinical condition characterized by concurrent appearance of physical frailty and mild cognitive impairments (MCI). Literature suggests common neuropathophysiological processes underlying physical and cognitive deficits, and physical dysfunction promotes cognitive decline, eventually leading to the emergence of Alzheimer's disease dementia. It remains to be discovered how neural activities and brain network reconfigurations are altered in the presence of physical frailty in MCI.

In the present study, [^{18}F]FDG PET and resting state fMRI scans were examined in 21 MCI patients without physical frailty (robust group: mean age = 74.7 ± 5.8 years) and 27 MCI with physical frailty (at-risk group: mean age = 75.5 ± 7.3 years). The first part of the study aimed to investigate changes in glucose metabolism and regional homogeneity in cognitive frailty. Regional cerebral

hypometabolism was observed in right frontal cortex, anterior cingulate, and bilateral superior parietal cortex in at-risk group, and the metabolic changes in left superior parietal cortex were associated with poorer performances in handgrip strength and executive function. Brain regional homogeneity was reduced in bilateral caudate, right medial and lateral frontal cortex, right superior temporal cortex, and cerebellum, and was increased in right precuneus and cerebellum. Decreased regional homogeneity in bilateral caudate and right superior temporal cortex showed correlations with weaker grip strength, slower gait speed, and lower physical activity, and the regional changes were also linked to cognitive performances in language and visuospatial function. The results demonstrated that the metabolic and functional alterations in cognitive frailty resembled Alzheimer's disease related pattern.

The second part of the study aimed to explore alterations in dynamic functional connectivity states and the temporal properties. Dynamic functional connectivity was measured using a sliding-window approach, and certain connectivity configurations (states) were estimated using *k*-means clustering method. Four distinguishing patterns of functional connectivity were found during the resting state scan time in our MCI cohorts. The most frequently occurring state (State 1) displayed mostly within-network connections, and the less occurring states (States 2, 3 and 4) displayed stronger between-network connections in both positive and negative fashions. The alterations in the temporal properties of dynamic states such as the number of transition, fractional windows, and mean dwell time of states did not reach the significance level, however, at-risk group appeared to have less reoccurrence of within-network State 1 and more reoccurrences of between-network States 2 and 3. Reduced reoccurrence and

shorter dwell time of within-network State 1 were significantly correlated with weaker handgrip strength, and the abnormally reduced within-network State 1 may reflect reduced functional network segregation coupled with physical deficits. On the other hand, higher reoccurrence and longer dwell time of State 2, which was characterized by heightened default mode network within-connectivity and increased interactions between default mode network and sensorimotor networks were associated with poorer MMSE-K score. The overexpression of interactions between default mode and sensorimotor networks may interfere with network functional specializations, leading to poor cognitive function. Furthermore, the functional connectivity strengths between sensorimotor and cognitive networks and within cognitive control network were altered in at-risk individuals.

The neuroimaging outcomes present that aberrant functional changes in frontal, temporal and parietal cortex may indicate advanced pathological process in the presence of physical frailty in MCI. The time-varying network reconfigurations indicating decreased functional segregation of brain networks may also serve as a potential biomarker in cognitive frailty.

Keywords: cognitive frailty, FDG PET, rs-fMRI, regional homogeneity, dynamic functional connectivity

Student Number: *2014-30671*

Contents

List of Figures

List of Tables

Chapter 1. Introduction

1.1 Frailty and cognition

Frailty is an age-related process which manifests as a reduction in physiological reserve and vulnerability to stressors, leading to increased adverse health-related outcomes such as disability, hospitalization, and mortality. Literature documented that physical frailty is associated with accelerated cognitive decline, involving memory, perceptual speed, and visuospatial cognitive systems (Boyle, Buchman, Wilson, Leurgans, & Bennett, 2010; Ruan et al., 2015). In a study of more than 750 community-based older persons from Rush Memory and Aging Project, for one-unit increase in frailty there was a 63 % increase in the risk of mild cognitive impairments (MCI) (Boyle et al., 2010). A prospective study by Gray et al. (2013) showed that frailty increased the likelihood of developing all-cause dementia to 1.2 times (to 1.08 times for Alzheimer's disease (AD)) in older adults over 65 years old. In Korean community-dwelling elderlies, it was found that age, a number of chronic diseases, depression, falls, hospitalization, cognitive deficits, and disability in instrumental activity of daily living were clearly linked to frailty, and frail subjects had higher risks of cognitive deficits, disability, falls, and hospitalization (Shim et al., 2011). Furthermore, in a large database study containing a total of 23,952 older individuals who aged over 65 years, over 40 % of the frailest group (15 % of the total) were diagnosed with dementia, while only 11 % were in the least frail group (60 % of the total) (Armstrong, Stolee, Hirdes, & Poss, 2010). Thereby, it is suggested that physical frailty and cognitive impairments may share

a common pathological mechanism, and they may be closely linked to higher risks of dementia (Ruan et al., 2015).

Cognitive frailty is proposed as a clinical syndrome in elderly population, which is determined by the presence of physical frailty and potentially reversible cognitive impairments (Clinical Dementia Rating (CDR) = 0.5) (Panza et al., 2006). Physical phenotypes of cognitive frailty are defined in terms of five components: poor handgrip strength, slow gait speed, a low level of physical activity, unintentional weight loss, and exhaustion (Fried et al., 2001). The presence of three or more of the features defines an individual as frail, and one or two features define as pre-frail. A consensus has reached on the definition of cognitive frailty by the International Academy on Nutrition and Aging and the International Association of Gerontology and Geriatrics (Kelaiditi et al., 2013). As previously described, physical frailty and cognition have an obvious relationship, and a growing body of evidence supports that cognitive frailty may be a prelude to dementia (Buchman, Boyle, Wilson, Tang, & Bennett, 2007; Ruan et al., 2015; Wilkins, Roe, Morris, & Galvin, 2013). It is thought that among the frailty components, grip strength and gait speed are the most powerful predictors of subsequent diagnosis of cognitive decline and MCI (Robertson, Savva, & Kenny, 2013). It remains to discover neural substrates of cognitive frailty and how frailty is related with dementia-related pathological processes.

Several neuroimaging evidence described structural changes in the brain of individuals with physical frailty (Avila-Funes et al., 2017; Jung et al., 2014a; Newman et al., 2001). For example, a disruption of white matter integrity in corpus callosum, internal capsule, external capsule, and thalamic radiations were reported in physically frail individuals (Avila-Funes et al., 2017). Also, frail subjects

showed a higher number of white matter lesions and increased ventricular size (Jung et al., 2014b; Newman et al., 2001). In recent neuroimaging studies in healthy older adults, phenotypes of frailty, specifically handgrip strength and walking speed were found to be associated with sensorimotor functional connectivity networks as well as with gray matter volumes in prefrontal cortex, basal ganglia, superior parietal cortex, and cerebellum (Rosano, Aizenstein, Studenski, & Newman, 2007; Seidler et al., 2015; Yuan, Blumen, Verghese, & Holtzer, 2015). Furthermore, it has been recognized that AD pathology promotes muscle weakness, motor impairment and frailty even in individuals with dementia (Buchman, Schneider, Leurgans, & Bennett, 2008; Buchman et al., 2014; Maltais et al., 2019), and a recent work reported deposition of cerebral amyloid-β, which is a biomarker of AD in potential sarcopenia (Wennberg et al., 2017). In agreement with the finding, accumulation of cerebral amyloid-β has been found to be linked to the presence of weakened grip strength in cognitive frailty (Yoon, Lee, Shin, Kim, & Song, 2018). The overall implies that alterations in the brain occur in frailty, which may contribute to the cognitive deterioration.

Up to the best of knowledge, no functional neuroimaging studies have yet been conducted in cognitive frailty. Understanding the underlying brain functional mechanisms may help untangle the relationships between physical and cognitive impairments in cognitive frailty. Thereby, prompt secondary intervention may achieve a better prognosis by targeting cognitively impaired patients with physical frailty for prevention of dementia.

1.2 Purpose of the study

The objective of the first part of the study is to explore regional metabolic and functional activity of the brain in cognitive frailty using [^{18}F]fluorodeoxy-D-glucose (FDG) positron emission tomography (PET) and resting state functional magnetic resonance imaging (rs-fMRI) measurements. The relationships between abnormal cerebral activities and phenotypes of physical frailty as well as cognitive function will be investigated.

In the second part of the study, dynamic changes of intrinsic functional network connectivity of the brain in cognitive frailty during the resting state scan will be evaluated and how the temporal properties of functional connectivity patterns are related to physical and cognitive performances will be addressed.

Chapter 2. Methodological Background

2.1 Measurement of cerebral glucose metabolism using [^{18}F]FDG PET

PET is a conventionally used medical imaging technique in nuclear medicine to assess biochemical processes. A radiolabeled [^{18}F]FDG is an analogue of glucose, and is taken up by activated cells in high demands of glucose for utilization. Thereby, the ligand uptake is indicative of the level of metabolic activity in the tissue. This underpins broad applications of [^{18}F]FDG PET imaging in detection and diagnosis of neurodegenerative diseases and cancer in medicine.

Metabolic pattern detected using [^{18}F]FDG PET already plays a significant role as a biomarker for diagnosis of different types of dementia (Ishii, 2014). Studies have also shown promising results on the prediction of developing dementia in MCI using [^{18}F]FDG PET. Chetelat et al. (2005) showed that [^{18}F]FDG PET measurement accurately predicts global cognitive deterioration at pre-dementia stage of AD better than neuropsychological assessments. In MCI who convert to AD, hypometabolism in temporo-parietal and medial frontal cortex is commonly found in lines of evidence (Arnaiz et al., 2001; Chetelat et al., 2003), and the same pattern of hypometabolism is also evident in early AD and in non-demented at-risk APOE-4 carriers (Haxby et al., 1990; Matsuda, 2001; Small et al., 2000).

In striking contrast, only a limited number of investigations about regional cerebral metabolic alterations in relation to physical performances have been conducted so far, most of them performed in physically normal older adults. In female older adults, low [^{18}F]FDG uptake in frontal and parietal cortices including

sensorimotor areas, prefrontal cortex, and cingulate in individuals was found to be associated with high step variability or with slower maximum gait speed (Sakurai et al., 2014; Shimada et al., 2013). With further investigations of metabolic activity alterations in cognitive frailty, we may gain better understanding of neural mechanisms underlying the relationship between physical and neurocognitive functions and relate to the emergence of AD in patients with cognitive frailty.

2.2 Measurements of brain functional activity and intrinsic network using rs-fMRI

2.2.1 Regional homogeneity using rs-fMRI

Rs-fMRI measures spontaneous neuronal activities in the brain, and offers means to assess brain functions and related functional networks at rest, specifically by measuring low-frequency oscillations of the fMRI time-series (0.01 - 0.1 Hz) (Biswal, Yetkin, Haughton, & Hyde, 1995; Biswal, Van Kylen, & Hyde, 1997; van den Heuvel & Hulshoff Pol, 2010).

One of data-driven methods in analyzing resting-state brain activity is a regional homogeneity (ReHo) method, which measures local synchronizations of a given voxel with those of its neighboring voxels in a temporal aspect (Zang, Jiang, Lu, He, & Tian, 2004). The method is based on the hypothesis that brain activities are likely to occur in a cluster of neighboring voxels rather than in a single voxel (Zang et al., 2004). Kendall's coefficient of concordance (KCC) is a widely employed measure of ReHo to represent the magnitude of functional coherence, and is assigned to each voxel, generating individual KCC maps (Kiviniemi et al., 2009). KCC can be calculated by:

$$KCC = \frac{\sum(Ri)^2 - n(\bar{R})^2}{\frac{1}{12}K^2(n^3 - n)}$$

where R_i is the sum rank of the ith time point, $\bar{R}$ is the mean of the R_i's, K is the number of time series within neighboring voxels, n is the number of ranks. KCC ranges from 0 to 1. The method has recently been used to characterize normal brain activity as well as pathological changes in many diseases (Shen et al., 2017; Wu et al., 2009; Yuan et al., 2016).

Functional studies using ReHo in cognitively impaired patients demonstrated aberrant spontaneous brain activity in regions including medial prefrontal cortex, posterior cingulate cortex, precuneus, temporal cortex, and inferior parietal lobule where are known to be primarily affected in MCI, and the altered ReHo was correlated with disease symptoms (Wang, Li, Yu, Huang, & Li, 2016; Wang et al., 2015b; Zhang et al., 2012). Mounting evidence of aberrant functional activity using ReHo has also been reported in AD (Marchitelli et al., 2018; Wang et al., 2017; Zhang et al., 2012). In contrast, no functional activation studies of ReHo have been applied to explore regional functional alterations in frailty. Since the rs-fMRI metrices are validated as potential biomarkers of neurodegenerative progresses (Albert et al., 2011), measurements of ReHo in older adults with cognitive frailty will provide insight to unravel the underlying neural mechanisms.

2.2.2 Group independent component analysis

It is established that the brain works as an integrative network, which is composed of subnetworks of anatomically separated, but temporally highly coherent (functionally connected) brain regions at rest. Among several techniques to

identify whole-brain functional connectivity patterns, a group independent component analysis (ICA) is the most commonly used method, which is model-free and shows a high level of consistency across many studies (van den Heuvel & Hulshoff Pol, 2010). The method searches for underlying sources (i.e. components) from a mixed signal (i.e. rs-fMRI time series), that are maximally independent from each other and explain different resting-state functional networks of brain regions (Calhoun, Liu, & Adali, 2009; van den Heuvel & Hulshoff Pol, 2010). The resting state networks that are consistently reported in ICA-based imaging studies are: visual network, motor network, attention network, salience network, default mode network (Corbetta & Shulman, 2002; Raichle et al., 2001; Seeley et al., 2007; van den Heuvel & Hulshoff Pol, 2010).

A common way to apply ICA to make group inferences in fMRI analysis is a group ICA approach, which temporally concatenates individual fMRI data to extract common independent components for group comparisons (Calhoun, Adali, Pearlson, & Pekar, 2001; Calhoun et al., 2009) (Figure 1). The procedure is then followed by a back-reconstruction process that allows to generate subject-specific spatial maps and time courses of independent components (Calhoun et al., 2001; Calhoun et al., 2009).

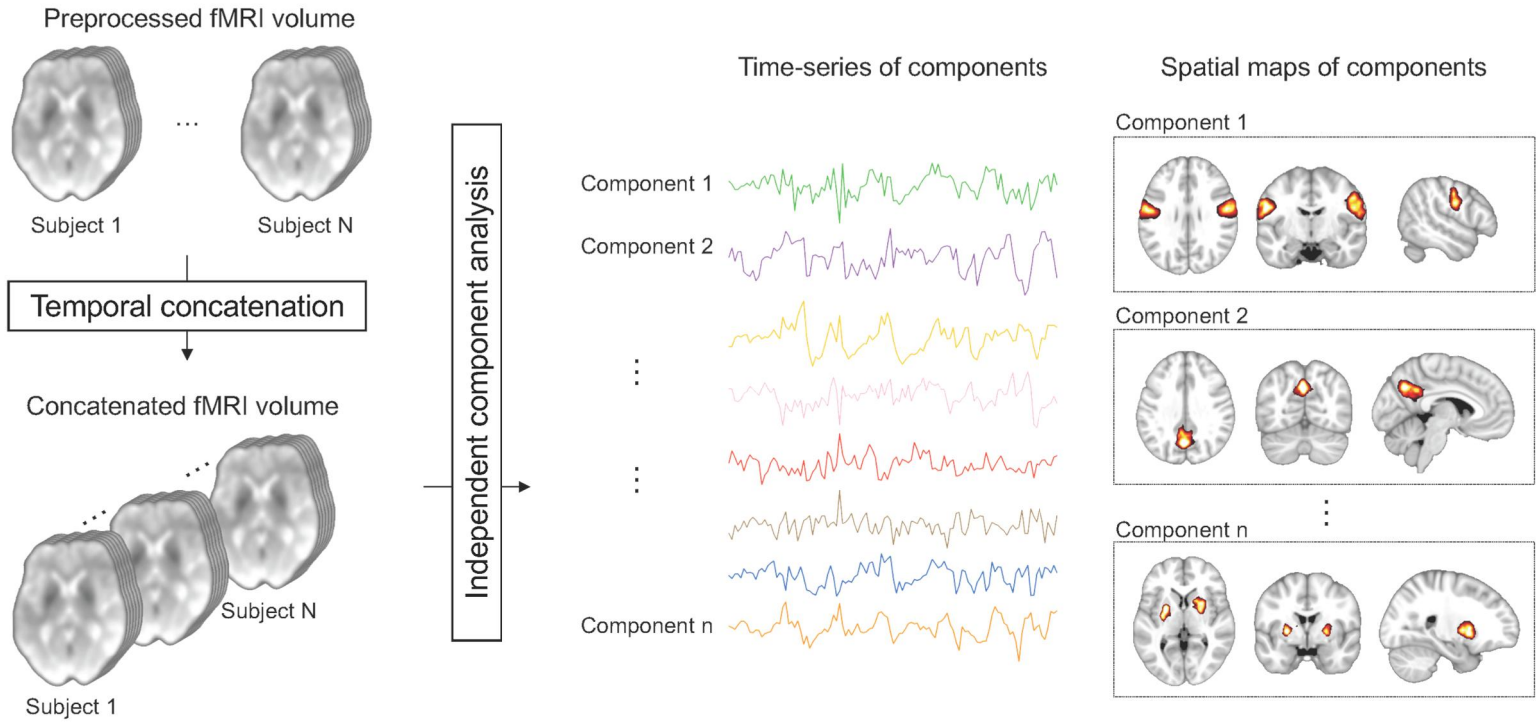

Figure 1. A schematic representation of group independent component analysis. (Abbreviations: fMRI = functional magnetic resonance image)

2.3 Dynamic functional connectivity analysis

Dynamic brain functional network analysis is a recent technique in rs-fMRI analysis, which explores temporal changes of resting-state brain network patterns during the scan time (Hutchison et al., 2013; Preti, Bolton, & Van De Ville, 2017). In the light of the novelty of the approach, the dynamic methods can provide information about neural communication beyond what is offered by static functional network analysis. In clinical implications, differences in neurocognitive activities may be present even if the static functional connectivity (in which functional activity is correlated in overall) appears to have similar variabilities between groups. Indeed, the strength and directionality of functional connectivity have shown to vary at fast time scales and even within the same subject between scans with the same imaging condition (Allen et al., 2014; Chang & Glover, 2010; Hutchison et al., 2013). Thereby, dynamic functional connectivity is thought to represent mental activity and cognitive function of individuals (Calhoun, Miller, Pearlson, & Adali, 2014; Thompson et al., 2013), and the approach has been applied in a number of studies to explore functional network features in relevance to symptoms and malfunctions in diseases such as Parkinson's disease, Schizophrenia, attention-deficit hyperactivity disorder, and dementias (Kaiser et al., 2016; Kim et al., 2017; Sourty et al., 2016; Viviano, Raz, Yuan, & Damoiseaux, 2017; Yu et al., 2015).

In order to compute temporal evolution of functional connections between brain regions, a sliding window technique is frequently used. Using the technique, the functional connectivity between a set of time courses of functional networks within a short segment (so called a window) of the scan time interval is calculated, and the same is repeated for subsequent segments until it spans the entire scan time

(Figure 2 (A)). Following calculations of time-varying functional connectivity matrices, the matrices are sorted to identify clusters of network configurations.

K-means clustering algorithm is a method to partition data into to a set of clusters while minimizing the within-cluster variance measured by the sum of least-squared distance (Lloyd, 1982). In the current study, the algorithm was applied to separate the dynamic functional connectivity matrices into a set of different clusters (states) (Figure 2 (B)). The occurrences and temporal features of observed functional connectivity states allow to examine the status of neural activity during the scan time, and they may also reflect functional roles in relations to cognition and disease symptoms (Allen et al., 2014; Kim et al., 2017).

In this study, dynamic functional network will be assessed based on the fore-mentioned methods, group ICA and a sliding window analysis. Dynamic functional connectivity will be measured by capturing correlations between component time courses using a series of sliding windows. After estimating the dynamic functional connectivity, *k*-means clustering approach will be used to identify reoccurring functional connectivity patterns.

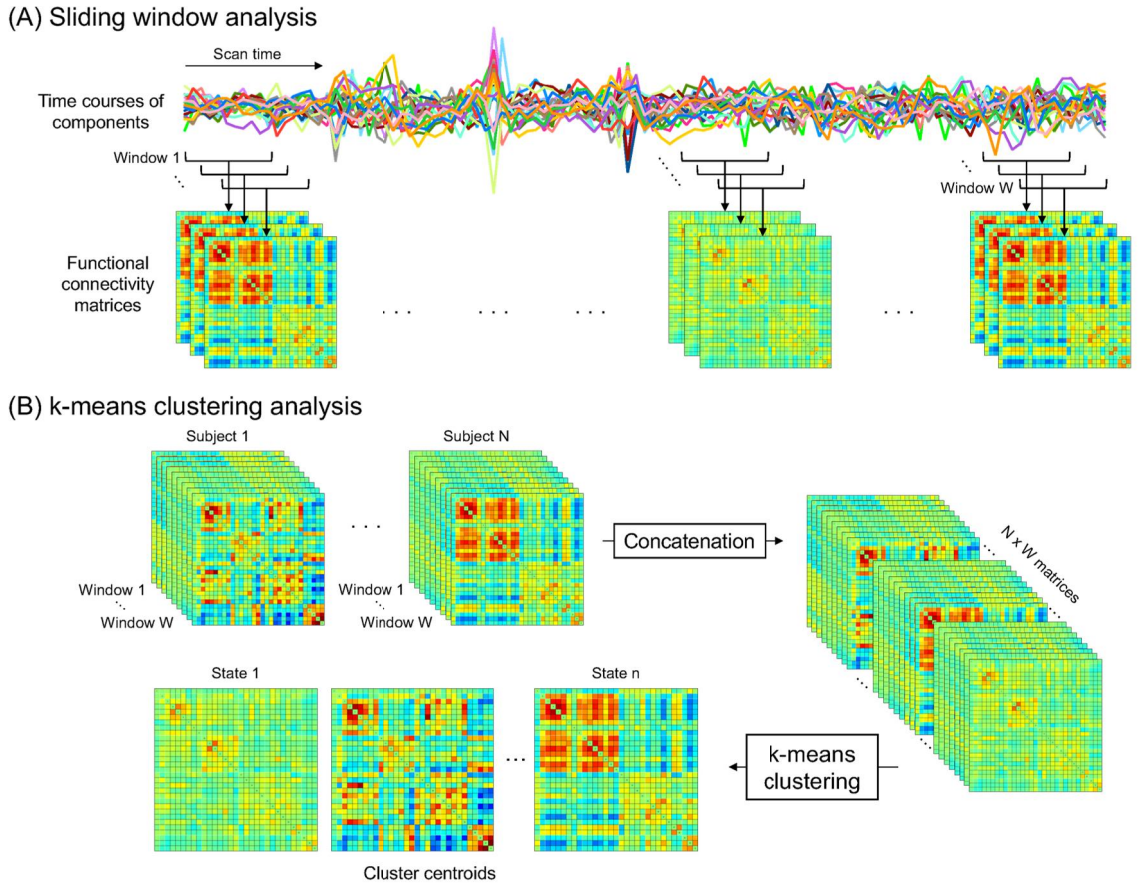

Figure 2. A schematic representation of dynamic functional connectivity analysis using (A) a sliding window approach and (B) *k*-means clustering approach.

Chapter 3. Subjects and Methods

3.1 Participants

3.1.1 Criteria of participants

Participants were recruited in Korean Brain Aging Study for Early Diagnosis and Prediction of Alzheimer's Disease (KBASE) study (Byun et al., 2017), where in MCI group included individuals who met the inclusion criteria of the NIA-AA guidelines (Albert et al., 2011). They had age of 55 - 90 years; memory complaint corroborated by self, an informant, or a clinician; objective memory impairment considering age, education, and gender; intact functional activities; no dementia. From the MCI group of KBASE study, fifty-nine subjects who were literate; aged 65 years or older; had no medical history of neuropsychiatric or neurologic disorders including depression and dementia; had no hospital admission in the past 12 months; were capable to walk at least 10-meters independently of the motility aid, were included in the current study. The participants underwent following cognitive and physical performance tests, and 11 were excluded due to low cognitive function (CDR greater than 1.0).

The participants were recruited from Seoul Metropolitan Government-Seoul National University Boramae Medical Center and two public centers for dementia prevention and management. The study protocol was approved by the Institutional Review Boards of Seoul National University Hospital (C-1401-027-547) and Seoul Metropolitan Government-Seoul National University Boramae Medical Center (26-2015-60), and all the procedures were completed in

accordance with the guidance of Helsinki Declaration. All the participants or their legal representatives provided an informed consent form.

3.1.2 Neuropsychological tests

Cognitive function of the participants was examined using a neuropsychological battery including the Korean version of the Consortium to Establish a Registry for Alzheimer's Disease (CERAD-K), Korean version of Mini-Mental State Examination (MMSE-K), CDR scales by a single rater for all subjects to minimize inter-rater bias. CERAD-K is comprised of five subtests derived from previously established tests: an executive domain of category verbal fluency test (24 points), a language domain of the Boston Naming Test (15 points), a memory domain of the Word List Learning test (30 points) with delayed recall (10 points) and recognition (10 points), and a visuospatial domain of the visual construction test (11 points). MMSE-K consists of orientation (10 points), short-term memory registration and recall (6 points), attention (5 points), naming (2 points), following verbal commands (4 points), judgement (2 points), and copying a double pentagon (1 point). CDR is made by interviewing a patient or a reliable informant such as a family member to characterize six cognitive domains: memory, orientation, judgement and problem solving, community affairs, home and hobbies, and personal care. The composite rating consists of five stages of dementia: 0 (no cognitive impairment), 0.5 (questionable), 1 (mild), 2 (moderate), and 3 (severe).

3.1.3 Physical frailty definition

Physical frailty was defined according to Fried criteria (Fried et al., 2001), and five frailty components were assessed: weight loss, weakness, exhaustion, slowness,

and physical activity. Weight loss was defined if one self-reported having unintentional weight loss of more than 4.5 kg in the past 12 months or when body mass index (BMI) was less than 18.5 kg/m^2. Weakness was defined as low handgrip strength considering the individual's gender and BMI. Grip strength was measured using a hand-to-hand dynamometer, and it repeated for four times for each participant with a short break in between. The average handgrip strength was calculated and compared to the cutoff point used in the Cardiovascular Health Study (CHS) (Fried et al., 1991). For males with BMI of ≤ 24, 24.1 - 26, 26.1 - 28, and > 28 kg/m^2, the cutoff points were ≤ 29, ≤ 30, ≤ 30, and ≤ 32 kg/m^2, respectively. For females with BMI of ≤ 23, 23.1 - 26, 26.1 - 29, > 29 kg/m^2, the cutoff points were ≤ 17, ≤ 17.3, ≤ 18, and ≤ 21 kg/m^2, respectively. Exhaustion was defined based on the questions from the Center for Epidemiologic Studies Depression Scale (CES-D) (Orme, Reis, & Herz, 1986): "How often have you felt that everything you had done was useless in the last week?" and "How often have you felt that you were not in the mood to do things you had to do in the last week?". The responses of "most of the time" and "often" were defined as the presence of exhaustion. Slowness was defined using the transit time a person takes to walk 4-meter distance in a straight line. and the criteria for frailty were set considering the gender and height. For male subjects, those who were shorter than 173 cm and had a timed walk > 7 s and those who were taller than 173 cm and had a timed walk > 6 s were defined as frail. For female subjects, those who were shorter than 159 cm and had a timed walk > 7 s and those who were taller than 159 cm and had a timed walk > 6 s were classified as frail. The low physical activity was assessed using International Physical Activity Questionnaire (IPAQ) (Craig et al., 2003), and three

levels of physical activity (high, moderate and low) were proposed, and responses describing low physical activity were indicated as frailty. Low activity described individuals who neither spent 3 or more days of vigorous activity of at least 20 minutes per day, 5 or more days of moderate intensity activity and/or walking of at least 30 minutes per day, or 5 or more days of any walking and moderate to vigorous activity achieving at least 600 MET-minutes/week (an index of metabolic energy expenditure). Participants were classified as frail when more than three criteria were met, pre-frail if one or two criteria were met, and robust if none of the criteria were met. Prefrail and frail individuals were grouped as at-risk group. Of 48 total subjects, 21 were in robust group, and 27 were in at-risk group. At-risk group included 25 pre-frail individuals and 2 frail individuals. Table 1 summarizes the five frailty criteria and cut point for each component.

Criterion	Frailty Status
Weight loss	**Frailty cut point:** Self reported unintentional weight loss > 4.5 kg in previous year Or BMI < 18.5 kg/m^2

Table 1. A summary of Fried criteria for frailty

Weakness	Measured using hand-to-hand dynamometer, average of 4 measures **Frailty cut point:** (the lowest 20 % by gender & BMI) Men *BMI* — *Cutoff* ≤ 24 — ≤ 29 24.1 - 26 — ≤ 30 26.1 - 28 — ≤ 30 > 28 — ≤ 32 Women *BMI* — *Cutoff* ≤ 23 — ≤ 17 23.1 - 26 — ≤ 17.3 26.1 - 29 — ≤ 18 > 29 — ≤ 21
Exhaustion	Center for Epidemiologic Studies Depression Scale: 1. "How often have you felt that everything you had done was useless in the last week?" 2. "How often have you felt that you were not in the mood to do things you had to do in the last week?" **Frailty cut point:** often, most of the time
Slowness	Timed walk over 4-meter distance **Frailty cut point:** Men *Height* — *Cutoff* ≤ 173 cm — ≥ 7 seconds >173 cm — > 6 seconds Women *Height* — *Cutoff* ≤ 158 cm — ≥ 7 seconds > 158 cm — > 6 seconds
Low physical activity	By International Physical Activity Questionnaire, in past week, spent either: • < 3 days of vigorous activity of at least 20 minutes/day • < 5 days of moderate intensity activity or walking of at least 30 minutes/day • < 5 days of any walking and moderate to vigorous activity achieving at least 60 MET-minutes/week **Frailty cut point:** the lowest 20 %

Frail: ≥ 3 criteria present; pre-frail: 1 or 2 criteria present; robust: 0 criteria present
Adapted from Fried et al. (2001) and modified
(Abbreviations: BMI = body mass index, MET = metabolic equivalent task)

3.1.4 Acquisition of [^{18}F]FDG PET and rs-fMR images

All participants underwent three-dimensional [^{18}F]FDG PET and MR imaging in a 3.0 Tesla Biograph mMR scanner on the same day (Siemens, Washington DC, USA). The participants fasted for at least 6 hours and rested in a waiting room for 40 minutes prior to the scans after intravenous administration of 0.1 mCi/Kg of [^{18}F]FDG PET radioligands. The PET data collected in list mode (5 minutes x 4 frames) were processed for routine corrections such as uniformity, UTE-based attenuation, and decay corrections. Following inspecting the data for any significant head movements, they were reconstructed into a 20-minute summed image using iterative methods (6 iterations with 21 subsets). [^{18}F]FDG PET images were acquired using the following imaging parameters: the number of slices, 127; matrix size, 344 mm x 344 mm; voxel size, 1.04 mm x 1.04 mm x 2.03 mm. The imaging acquisition parameters for rs-fMRI were: the number of total functional volume, 116; the number of slices, 45; matrix size, 128 mm x 128 mm; voxel size, 1.88 mm x 1.88 mm; slice thickness, 3.0 mm; repetition time (TR), 3000 ms; echo time, 30 ms; flip angle, 90°. The images were acquired in a resting state condition with dimmed light and subject's eyes closed. For the purposes of coregistration and accurate spatial normalization of [^{18}F]FDG PET image and assessment of structural lesions in the subjects, structural T1 images were obtained in sagittal acquisition using the following scanning parameters: the number of slices, 208; matrix size, 256 mm x 256 mm; voxel size, 0.98 mm x 0.98 mm x 1.0 mm; repetition time, 1670 ms; echo time, 1.89 ms; inversion time, 900 ms, flip angle, 9°.

3.1.5 Statistical analysis

Statistical analyses were performed using SPSS 13.0 (IBM Corporation, Chicago, IL) for demographic and clinical variables of subjects. The variables were compared between the groups using chi-square test for categorical variables (gender distribution and frailty phenotypes) and independent sample t-test for continuous variables (age, years of education, BMI, MMSE-K, and CERAD-K scores). The variables were considered significantly different between groups if p-value < 0.05.

3.2 [^{18}F]FDG PET image analysis

3.2.1 Preprocessing steps of [^{18}F]FDG PET

The image preprocessing steps were performed using SPM 12 (Statistical Parametric Mapping) software implemented on Matlab 2018b (Mathworks, http://www.mathworks.com). Static PET images were coregistered to individual structural T1 image, and spatially normalized to a standard Montreal Neurological Institute (MNI) space. The images were then smoothed with a Gaussian filter of 8-mm full-width-at-half-maximum (FWHM) for group comparisons. Figure 3 illustrates the preprocessing steps for [^{18}F]FDG PET images.

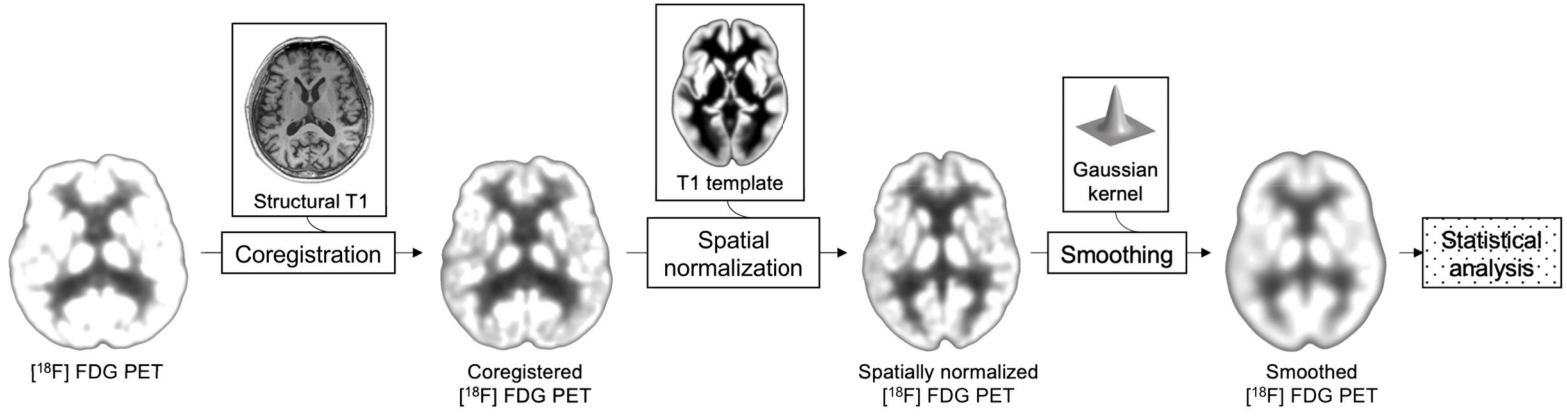

Figure 3. A schematic representation of preprocessing procedures for [^{18}F]FDG PET images. (Abbreviations: FDG = fluorodeoxyglucose, PET = positron emission tomography)

3.2.2 Statistical analysis

Brain glucose metabolism measured using [^{18}F]FDG PET images were compared between the groups in a voxel-wise manner using two-sample t-test with age, gender, and years of education added as covariates. The results were considered statistically significant if uncorrected p-value < 0.005 and cluster size > 20 contiguous voxels.

A stepwise multiple regression analysis was employed to identify brain regions with abnormal metabolism changes relevant to frailty phenotypes and cognitive performances.

3.3 Resting state functional MRI analysis

3.3.1 Preprocessing steps of rs-fMRI

Functional MRI data were preprocessed using DPARSFA (Data Processing Assistant for Resting-State fMRI, advanced version 4.3) and SPM 12. First of all, the first five volumes were discarded to ensure magnetization equilibrium. The functional data were then corrected for slice timing differences using the middle volume as a reference, and spatially realigned to the middle slice using a least-squares approach and six parameter rigid body spatial transformations. The realigned functional images were spatially normalized to MNI space using EPI template, and then the images were smoothed with a Gaussian kernel of 6-mm-FWHM. Of the total forty-eight subjects, two were excluded from further analyses due to head movements greater than 2.0 mm and 2.0 degrees in any dimension during the scans. In Figure 4, the preprocessing procedures for rs-fMRI data are summarized.

3.3.2 Calculations of regional homogeneity

The calculations of ReHo maps were performed using DPARSF and SPM 12. The preprocessed rs-fMRI images prior to smoothing from Section 3.3.1 were processed by regressing out six motion parameters and averaged time courses of white matter and cerebrospinal fluids, and applying temporal band-pass filtering at 0.01 - 0.1 Hz. To generate individual ReHo maps, KCC for every voxel with its neighboring 26 voxels was calculated in a voxel-wise manner.

3.3.3 Statistical analysis

The individual ReHo maps were compared between the groups using a two-sample t-test, and the results were thresholded at uncorrected $p < 0.005$ and cluster size > 10 voxels. Age, gender, and years of education were entered as covariates of no interest. The results were further examined for correlations between functional activity abnormalities and physical and cognitive performances using stepwise multiple regression analysis.

3.4 Functional connectivity analysis using rs-fMRI

3.4.1 Group independent component analysis

Prior to group independent component analysis (ICA), the preprocessed rs-fMRI images were normalized by Fisher's z-transformations. The rs-fMRI data were decomposed into networks using a group-level spatial ICA using GIFT toolbox (version 3.01, http://icatb.sourceforge.net). The data were decomposed into a set of spatially independent components (IC, IC = 50) using a higher-order ICA approach to promote anatomical and functional parcellations, as has been implemented in previous functional network studies (Allen et al., 2014; Kim et al., 2017; Kiviniemi

et al., 2009). In a subject-specific data reduction step, 75 principal components were retained using principal component analysis, and in the group level data reduction, the concatenated subject data were decomposed into 50 components using the expectation maximization algorithm. The reliability of Infomax ICA algorithm was evaluated by iterating the estimations 20 times using ICASSO implemented in GIFT. To generate subject-specific spatial maps and time courses for each IC, the group IC's were back-reconstructed using GICA back reconstruction method.

Of the 50 IC's, 31 components were identified as meaningful brain functional networks based on the following criteria: (a) the peak activations are located in gray matter, (b) low spatial overlaps are observed with physiological, motion, or imaging artefacts, (c) the time courses are dominated by low-frequency fluctuations (Allen et al., 2014). The selected 31 components were further categorized into seven functional networks: basal ganglia (BG), auditory (AUD), somatomotor (SM), visual (VIS), cognitive control (CC), default mode (DM), and cerebellar (CB) networks.

Finally, the component time courses underwent additional processing steps to remove noises: detrending, despiking, low-pass filtering with a cutoff of 0.15 Hz, and regression of the six realignment parameters.

3.4.2 Dynamic functional network connectivity analysis

Temporal dynamic functional network analysis was performed using dFNC toolbox (version 1.0a) in GIFT, using a sliding window approach and *k*-means clustering algorithm. In a sliding window approach, the time series was segmented into 15-TR (45 s) long windows convolved with a Gaussian (σ = 2 TRs), and the

window was slid in steps of 1-TR along the scan, resulting in 96 consecutive windows. Thereby, time-varying changes of functional connectivity patterns of 31 independent components during the length of scan at rest were examined. The covariance matrix between the components was estimated from the regularized precision matrix (inverse covariance matrix). In order to promote sparsity in the estimation of the matrix, an L1 penalty was imposed in the graphical LASSO method (Friedman, 2007), and the L1 regularization was repeated 100 times. The dynamic functional connectivity matrices were converted by Fisher's z-transforms to normalize the variance for further analysis. The functional connectivity matrices were also residualized with confounding factors (age, gender, and years of education).

Functional connectivity patterns which reoccur during the resting state scan were assessed using *k*-means clustering algorithm applied to the 96 windowed covariance matrices. For the high-dimensional data, L1 distance (city block distance/Manhattan distance) function was used to measure the similarity between each functional connectivity matrix and the cluster centroid. Prior to clustering, the data were subsampled to reduce the redundancy between consequent windows which show a high autocorrelation with a short time step of 1 TR, and to minimize computational loads. The clustering algorithm was applied with 500 iterations with random initializations of cluster centroid positions. In order to determine the optimal number of clusters (*k*), the elbow criterion of the cluster validity index was employed, which studies the percentage of variance over a range of the number of clusters and chooses the optimal number so that adding another does not improve the within-cluster sum of square much better. The optimal *k* (will be referred to states from this point) found in the current work was four. The individual

functional connectivity matrices were divided into the four states based on the similarity with the cluster centroids. A state transition vector which represents individual's dynamic changes of functional connectivity state status and characterizes temporal properties of the state was obtained. The variables to characterize the temporal properties of dynamic functional connectivity states were: the number of state transitions, fractional windows, and mean dwell time. The number of transitions represents how many times an individual changed from one state to another during the scan time, and a higher number of transitions reflects more dynamic changes (or less stability) of network connectivity over time. The fractional window is the proportion of time spent in each state during the scan. The mean dwell time measures the average of time lengths (in units of windows) an individual stayed in one state without changing to another once entered the state.

3.4.3 Reproducibility analyses of dynamic functional connectivity states

First of all, additional exploratory analyses were performed by applying the clustering algorithm for a range of k from 2 to 8 to confirm the robustness of the functional connectivity patterns and relative reoccurrences of the states regarding different values of k. The clustering algorithm was repeated 500 times for each k value. In addition to that, reproducibility of clusters was also established by repeating the clustering procedure to 200 bootstrap resampled datasets. Each bootstrap resampled dataset consisted of 46 randomly sampled subjects' data with replacement, and the clustering analysis was conducted for each dataset with 500 iterations. For cluster centroids found for each bootstrap dataset, the similarity was measured by calculating a city block distance from the cluster centroids for original

data, and the cluster centroids were assigned to the state index with the closest distance. The centroids with assigned state indices were also visually inspected.

3.4.4 Graph theory-based topological analysis: network efficiency

A topological graph theory analysis was applied to explore variability in dynamic functional organizations using GRETNA software (A Graph Theoretical Network Analysis Toolbox version 2.0, http://www.nitrc.org/projects/gretna). In order to remove confounding effects of spurious correlations in the matrices, a sparsity threshold was firstly defined. The sparsity threshold is the ratio of the number of actual edges divided by the maximum possible number of edges in a network, and a range of the sparsity threshold from 0.1 to 0.4 in increments by 0.01 was applied to the 96 dynamic functional connectivity matrices. The matrices were then binarized by assigning 1 to edges greater than the threshold and 0 otherwise. Only positive relationships were considered in the analysis. Two topological variables, global efficiency and local efficiency were calculated to analyze efficiency of information transfer in a network at each sparsity threshold. Global efficiency (E_{glob}) of a network G with number N of nodes is calculated by:

$$E_{glob}(G) = \frac{1}{N(N-1)} \sum_{i \neq j \in G} \frac{1}{d_{ij}}$$

where d_{ij} is the shortest path length between nodes i and j. Local efficiency (E_{loc}) can be calculated by:

$$E_{loc}(G) = \frac{1}{N} \sum_{i \in G} E_{glob}(G_i)$$

Global efficiency represents the efficiency of parallel information transfer in the whole brain network, and local efficiency measures the efficiency of information transfer among the direct neighbors of a given node.

3.4.5 Statistical analysis

Group differences in the temporal properties of dynamic functional connectivity were examined using non-parametric Mann-Whitney U test, and a statistical threshold of $p < 0.05$ was applied. The relationships between the variables of dynamic functional connectivity state analysis with frailty measures (handgrip strength, average timed walk, and IPAQ physical activity level) as well as with cognitive data were explored using a stepwise multiple regression analysis, after controlling for age, gender, and years of education. Furthermore, the functional connectivity strengths in each state were compared between robust and at-risk groups using two-sample t-test (uncorrected p-value < 0.001). The functional connectivity strengths with group differences were assessed for relationships with physical and cognitive performances using a general linear model. The same p-value threshold of 0.05 was applied for statistical significance.

For graph theory-based network analysis, the area under curve (AUC) within the defined sparsity threshold range was calculated for each network measure, which provides a scalar for analyses that do not depend on selection of a single specific threshold. The variability of global and local efficiency across the resting scan was assessed by calculating the interquartile range of AUC changes, and compared between groups. A correlation analysis was also performed to test whether physical performances affect the variability of network efficiencies.

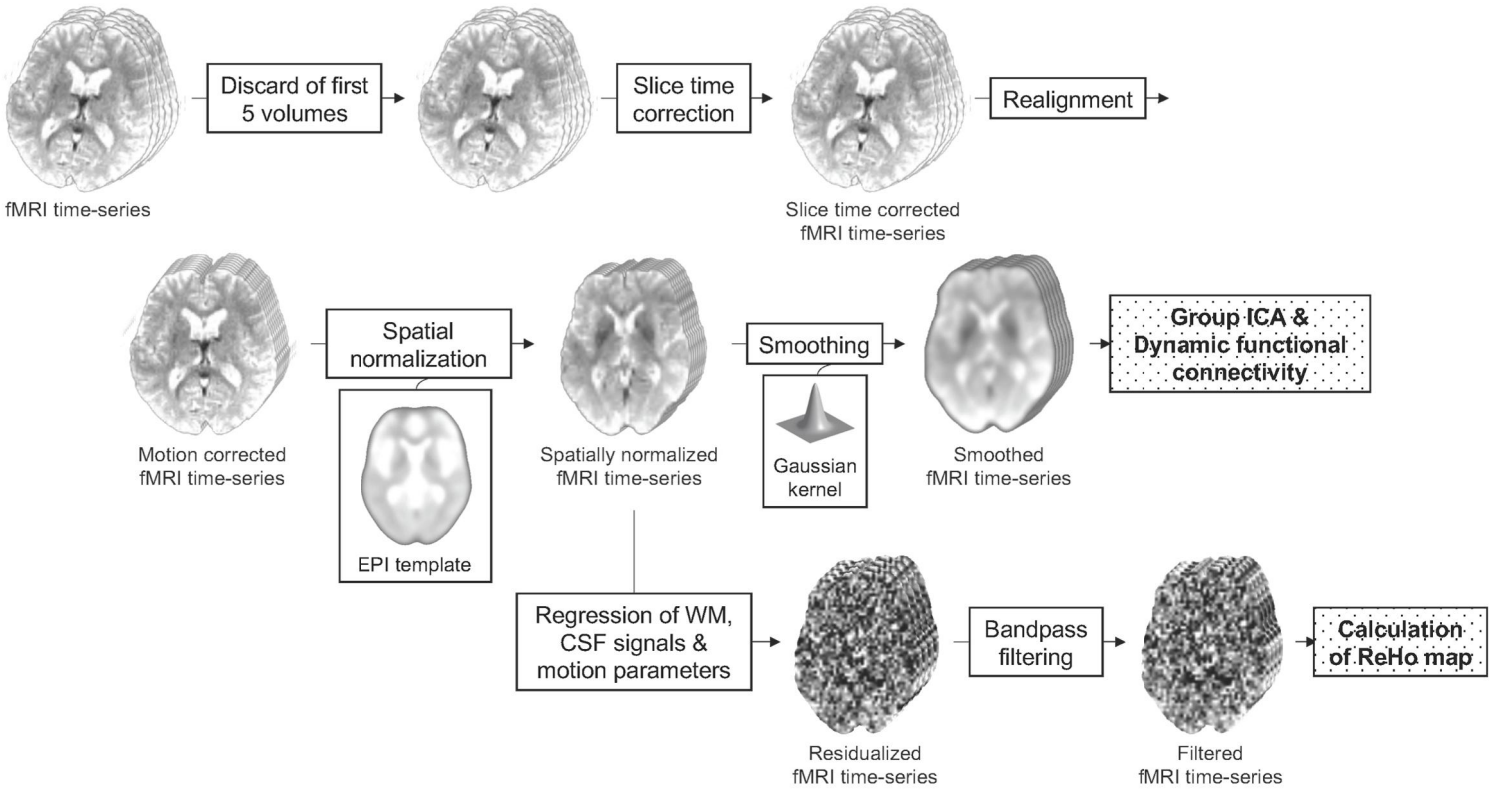

Figure 4. A schematic representation of preprocessing procedures for resting state fMRI images. (Abbreviations: fMRI = functional magnetic resonance image, EPI = echo planar image, WM = white matter, CSF = cerebrospinal fluid, ICA = independent component analysis, ReHo = regional homogeneity)

Chapter 4. Results

4.1 Demographic and clinical characteristics of robust and at-risk groups

There were no significant differences in age, gender distribution, years of education, BMI, MMSE-K, and CERAD-K scores between at-risk and robust groups, except for executive function (verbal fluency). The group differences in frailty criteria were evident in the presence of exhaustion, low physical activity, and weakness ($p = 0.014$, < 0.001, and < 0.001, respectively, using chi-square test). Detailed information on demographic features and physical and cognitive performances of subjects is summarized in Table 2.

Table 2. Demographic features and physical cognitive performances of subjects

	Robust (n = 21)	**At-risk (n = 27)**	***p*-value**
Age	74.7 (5.8)	75.5 (7.3)	0.681
Gender ratio, male %	38 %	26 %	0.531†
Years of education	9.3 (4.2)	9.7 (4.3)	0.760
Body mass index	25.3 (2.6)	24.7(4.0)	0.527
MMSE-K	24.5 (2.3)	24.0 (2.2)	0.436
CERAD-K total score	59.4 (10.8)	56.6 (9.6)	0.355
Memory	24.2 (5.9)	25.4 (5.6)	0.503
Construction	10.1 (1.4)	9.3 (1.4)	0.053
Executive function	14.9 (4.7)	12.1 (4.3)	*0.036**
Language	10.1 (2.4)	9.9 (2.5)	0.816
Frailty criteria, n			
Weight loss	0	4	0.121†
Exhaustion	0	7	*0.014*†*
Low physical activity (mean (std))	0 (2416.5 (1468.4))	11 (1430.7 (1290.8))	*0.001*†*
Weakness (mean (std) unit)	0 (27.2 (7.2) kg)	13 (21.2 (3.7) kg)	< *0.001*†*
Slowness (mean (std) unit)	0 (4.5 (0.7) s)	4 (5.9 (4.0) s)	0.121†

Values are means (standard deviations)
† Using chi-square test (Otherwise, *p*-values are calculated using independent sample t-test)
* Significant at *p*-value < 0.05
(Abbreviations: MMSE-K = Korean version of Mini-Mental State Examination, CERAD-K = Korean version of the Consortium to Establish a Registry for Alzheimer's Disease, std = standard deviation)

4.2 Glucose metabolism using [^{18}F]FDG PET

4.2.1 Group comparison in glucose metabolism

In at-risk group, glucose metabolism decreased in bilateral superior parietal lobule, right frontal cortex and anterior cingulate cortex in comparison to robust group (Figure 5, Table 3). No increases in glucose metabolism were observed.

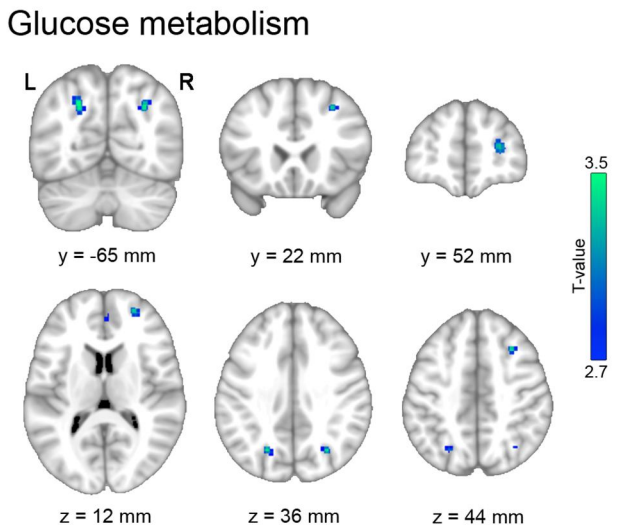

Figure 5. Changes in glucose metabolism in at-risk group compared to robust group. Cool color indicates decreased glucose metabolism in at-risk group. (Abbreviations: L = left, R = right)

Table 3. Brain regions with changes in glucose metabolism in at-risk group

	Brain region	k	T-value	x	y	z
Robust < At-risk	None					
Robust > At-risk	Superior parietal lobule, L	65	3.51	-22	-66	38
	Middle frontal cortex, R	27	3.47	30	20	44
	Superior parietal lobule, R	42	3.46	30	-66	38
	Middle frontal cortex, R	62	3.45	28	54	10
	Anterior cingulate, R	22	2.92	2	46	10

The coordinates are the peak activation in Montreal Neurological Institute space from two-sample t-test for comparison of brain glucose metabolism between groups at uncorrected *p*-value < 0.005 and cluster extent size (k) > 20 voxels. (Abbreviations: L = left, R = right)

4.2.2 Relationships between cerebral glucose metabolism and physical and cognitive performances

A step-wise multiple regression analysis showed that hypometabolism in left superior parietal cortex was significantly associated with weaker handgrip strength (standardized $\beta = 0.314$, $p = 0.036$) and poorer performance in executive function ($\beta = 0.289$, $p = 0.043$). Interaction effects between frailty and cognitive data on the regional metabolic change were not significant. The results are summarized in Table 4, and Figure 6 displays partial correlations between the regional metabolic activity and physical and cognitive performance.

Table 4. Multiple regression analysis results for physical and cognitive performances associated with regional glucose metabolism changes

			Adj. R^2	β	*p*	VIF
Superior parietal cortex, L						
Physical performance	Single (enter)	Grip strength *	0.101	0.347	0.016	
		Timed walk	0.006	-0.165	0.268	
		Physical activity	-0.018	-0.062	0.680	
		Weight loss	-0.011	-0.105	0.480	
		Exhaustion	0.004	-0.160	0.277	
	Multiple (stepwise)	Grip strength *	0.120	0.374	0.011	1.000
		Timed walk		-0.050	0.740	1.140
		Physical activity		-0.160	0.277	1.086
		Weight loss		-0.083	0.559	1.000
		Exhaustion		-0.093	0.520	1.048
Cognitive performance	Single (enter)	Memory	-0.004	-0.131	0.374	
		Visuospatial	0.042	0.251	0.086	
		Executive *	0.100	0.345	0.016	
		Language	-0.021	-0.034	0.817	
		MMSE-K	-0.009	-0.110	0.457	
	Multiple (stepwise)	Executive *	0.100	0.345	0.016	1.000
		Memory		-0.235	0.101	1.070
		Visuospatial		0.256	0.064	1.000
		Language		-0.166	0.262	1.121
		MMSE-K		-0.243	0.096	1.111
Physical & Cognitive performances	Multiple (stepwise)	Grip strength *	0.154	0.314	0.036	1.165
		Executive *		0.289	0.043	1.065
		Strength x Executive		-0.044	0.760	1.153

Asterisks indicate significant results at *p*-value < 0.05. (Abbreviations: L = left, Adj. R^2 = adjusted R^2, VIF = variance inflation factor)

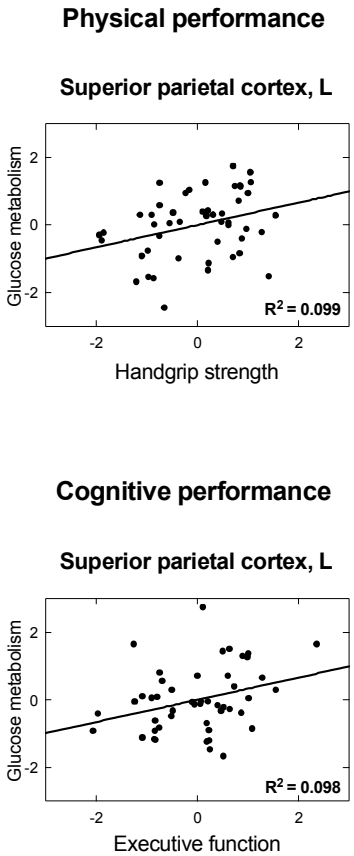

Figure 6. Plots of significant correlations between regional glucose metabolism and physical (above) and cognitive (below) performances (Abbreviations: L = left)

4.3 Resting-state functional activity using regional homogeneity

4.3.1 Group comparison in regional homogeneity

As shown in Figure 7 and Table 5, reductions in ReHo were observed in bilateral caudate, right superior temporal cortex, left cerebellum, right fusiform gyrus, and right frontal cortex in at-risk group. On the other hand, abnormal increases in ReHo were found in left cerebellum and right precuneus.

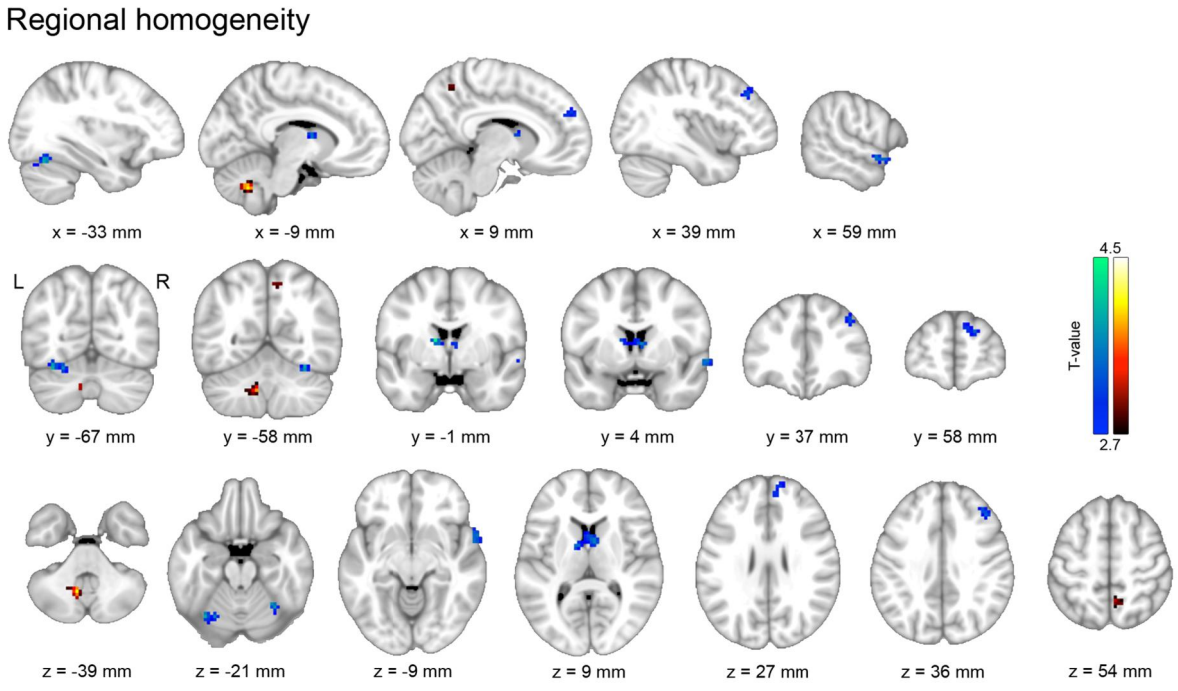

Figure 7. Changes in regional homogeneity in at-risk group compared to robust group. Warm color indicates increases in at-risk group, and cool color indicates decreases. (Abbreviations: L = left, R = right)

Table 5. Brain regions with changes in regional homogeneity in at-risk group

	Brain region	k	T-value	x	y	z
Robust < At-risk	Cerebellum, L	28	4.01	-9	-60	-39
	Precuneus, R	10	3.18	6	-54	54
Robust > At-risk	Caudate, L	46	4.45	-12	0	12
	Caudate, R		3.59	6	3	9
	Cerebellum, L	39	3.92	-33	-66	-21
	Cerebellum, L		3.62	-24	-66	-21
	Cerebellum, L		3.02	-42	-69	-24
	Fusiform cortex, R	16	3.86	33	-57	-18
	Superior temporal cortex, R	20	3.56	63	3	-6
	Superior frontal cortex, R	29	3.37	18	57	24
	Superior frontal cortex, R		3.16	9	54	30
	Superior frontal cortex, L		3.06	0	48	21
	Middle frontal cortex, R	20	3.36	42	30	36

The coordinates are the peak activation in Montreal Neurological Institute space from two-sample t-test for comparison of brain regional homogeneity between groups at uncorrected *p*-value < 0.005 and cluster extent size (k) > 10 voxels. (Abbreviations: L = left, R = right)

4.3.2 Relationships between regional homogeneity and physical and cognitive performances

A multiple regression analysis showed that reduced ReHo in bilateral caudate was significantly associated with weaker handgrip strength ($\beta = 0.387$, $p = 0.007$), longer timed walk ($\beta = -0.312$, $p = 0.021$), and poorer performance in language ($\beta = 0.280$, $p = 0.036$). ReHo in right superior temporal cortex decreased with weaker handgrip strength ($\beta = 0.310$, $p = 0.029$), lower level of physical activity ($\beta = 0.274$, $p = 0.047$), and poorer visuospatial function ($\beta = 0.341$, $p = 0.009$). On the other hand, increasing ReHo in right precuneus was associated with weaker handgrip strength ($\beta = -0.324$, $p = 0.025$) and memory function ($\beta = 0.308$, $p = 0.032$). No significant interactions between physical and cognitive data with main effects were observed. Table 6 summarizes the results of stepwise multiple regression analysis, and Figure 8 shows partial correlation plots between ReHo and physical/cognitive performances.

Table 6. Multiple regression analysis results for physical and cognitive performances associated with regional homogeneity changes

			Adj. R^2	β	*p*	VIF
Caudate, Bilateral						
Physical performance	Single (enter)	Grip strength *	0.233	0.500	< 0.001	
		Timed walk *	0.196	-0.463	0.001	
		Physical activity *	0.071	0.302	0.041	
		Weight loss	-0.022	0.023	0.878	
		Exhaustion	-0.022	-0.025	0.869	
	Multiple (stepwise)	Grip strength *	0.319	0.393	0.005	1.137
		Timed walk *		-0.326	0.018	1.137
		Physical activity		0.118	0.371	1.098
		Weight loss		0.065	0.610	1.022
		Exhaustion		0.117	0.367	1.054
Cognitive performance	Single (enter)	Memory	-0.019	0.062	0.681	
		Visuospatial	0.019	0.202	0.177	
		Executive *	0.065	0.292	0.049	
		Language *	0.096	0.340	0.021	
		MMSE-K	-0.016	0.082	0.589	
	Multiple (stepwise)	Language *	0.096	0.340	0.021	1.000
		Memory		-0.031	0.834	1.078
		Visuospatial		0.164	0.254	1.014
		Executive		0.203	0.177	1.117
		MMSE-K		0.044	0.761	1.013
Physical & Cognitive performances	Multiple (stepwise)	Grip strength *	0.362	0.387	0.007	1.267
		Timed walk *		-0.312	0.021	1.166
		Language *		0.280	0.036	1.145
		Strength x Language		0.014	0.925	1.462
		Speed x Language		-0.058	0.675	1.310
Superior temporal cortex, R						
Physical performance	Single (enter)	Grip strength *	0.160	0.423	0.003	
		Timed walk	0.005	-0.166	0.276	
		Physical activity *	0.145	0.405	0.005	
		Weight loss	-0.020	0.053	0.725	
		Exhaustion	-0.012	-0.102	0.501	
	Multiple (stepwise)	Grip strength *	0.228	0.333	0.020	1.090
		Physical activity *		0.305	0.033	1.090
		Timed walk		0.004	0.979	1.145
		Weight loss		0.044	0.746	1.000
		Exhaustion		-0.009	0.945	1.046
Cognitive performance	Single (enter)	Memory	0.003	0.158	0.294	
		Visuospatial *	0.152	0.414	0.004	

		Executive	-0.007	0.125	0.406	
		Language	-0.001	0.145	0.337	
		MMSE-K	-0.019	0.058	0.701	
	Multiple (stepwise)	Visuospatial *	0.152	0.414	0.004	1.000
		Memory		0.056	0.698	1.070
		Executive		0.137	0.322	1.001
		Language		0.097	0.488	1.014
		MMSE-K		-0.040	0.778	1.057
Physical & Cognitive performances	Multiple (stepwise)	Grip strength *	0.324	0.31	0.029	1.249
		Physical activity *		0.274	0.047	1.196
		Visuospatial *		0.341	0.009	1.041
		Strength x Visuospatial		0.145	0.285	1.187
		Activity x Visuospatial		-0.025	0.852	1.172
Precuneus, R						
Physical performance	Single (enter)	Grip strength *	0.125	-0.380	0.009	
		Timed walk	-0.001	0.149	0.328	
		Physical activity *	0.092	-0.335	0.023	
		Weight loss	-0.017	0.075	0.621	
		Exhaustion	-0.006	0.130	0.390	
	Multiple (stepwise)	Grip strength *	0.123	-0.378	0.011	1.000
		Timed walk		0.021	0.893	1.137
		Physical activity		-0.232	0.116	1.090
		Weight loss		0.081	0.574	1.000
		Exhaustion		0.052	0.721	1.045
Cognitive performance	Single (enter)	Memory *	0.067	0.297	0.045	
		Visuospatial	-0.020	-0.051	0.734	
		Executive	-0.001	0.145	0.336	
		Language	0.038	0.195	0.195	
		MMSE-K	-0.019	0.061	0.687	
	Multiple (stepwise)	Memory *	0.067	0.297	0.045	1.000
		Visuospatial		-0.136	0.367	0.935
		Executive		0.056	0.718	0.897
		Language		0.124	0.413	0.928
		MMSE-K		-0.123	0.471	0.739
Physical & Cognitive performances	Multiple (stepwise)	Grip strength *	0.186	-0.324	0.025	1.075
		Memory *		0.308	0.032	1.061
		Strength x Memory		-0.154	0.284	1.119

Asterisks indicate significant results at p-value < 0.05. (Abbreviations: R = right, MMSE-K = Korean version of Mini-Mental State Examination, Adj. R^2 = adjusted R^2, VIF = variance inflation factor)

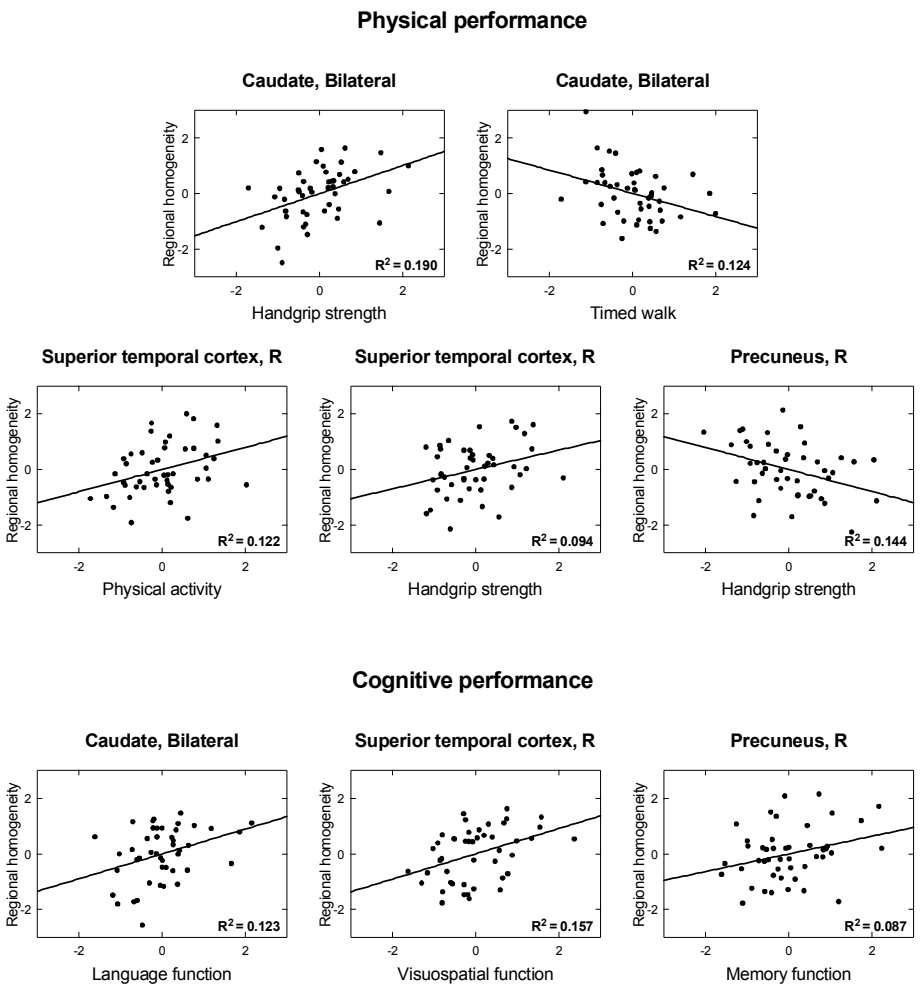

Figure 8. Plots of significant correlations between regional homogeneity and physical (above) and cognitive (below) performances. (Abbreviations: L = left, R = right)

4.4 Dynamic functional connectivity of brain networks

4.4.1 Functional connectivity networks

Figure 9 displays spatial maps of independent components identified using group ICA and classified into seven functional networks. BG network consists of IC 30, and AUD network consists of IC 33. SM network consists of ICs 2, 3, 4, 6, 29, 32, and 39, and VIS consists of ICs 1, 5, 9, 27, 40, 49, and 50. CC network included ICs 12, 19, 28, 35, and 45, and DM network included ICs 8, 10, 16, 17, 18, 34, and 38. CB network included ICs 11, 14, 26. Details on brain region name, T-value and coordinates of peak activation, and size of clusters obtained by using one-sample t-test for each component are listed in Table 7 (family-wise error corrected $p < 0.01$, cluster size > 100 contiguous voxels).

Figure 10 displays the averaged static functional connectivity matrix between independent components of the functional networks across the subjects. Positive within-network functional connectivity is observed, while weak or even negative connectivity is observed between two different functional networks, as previously observed (Allen et al., 2014).

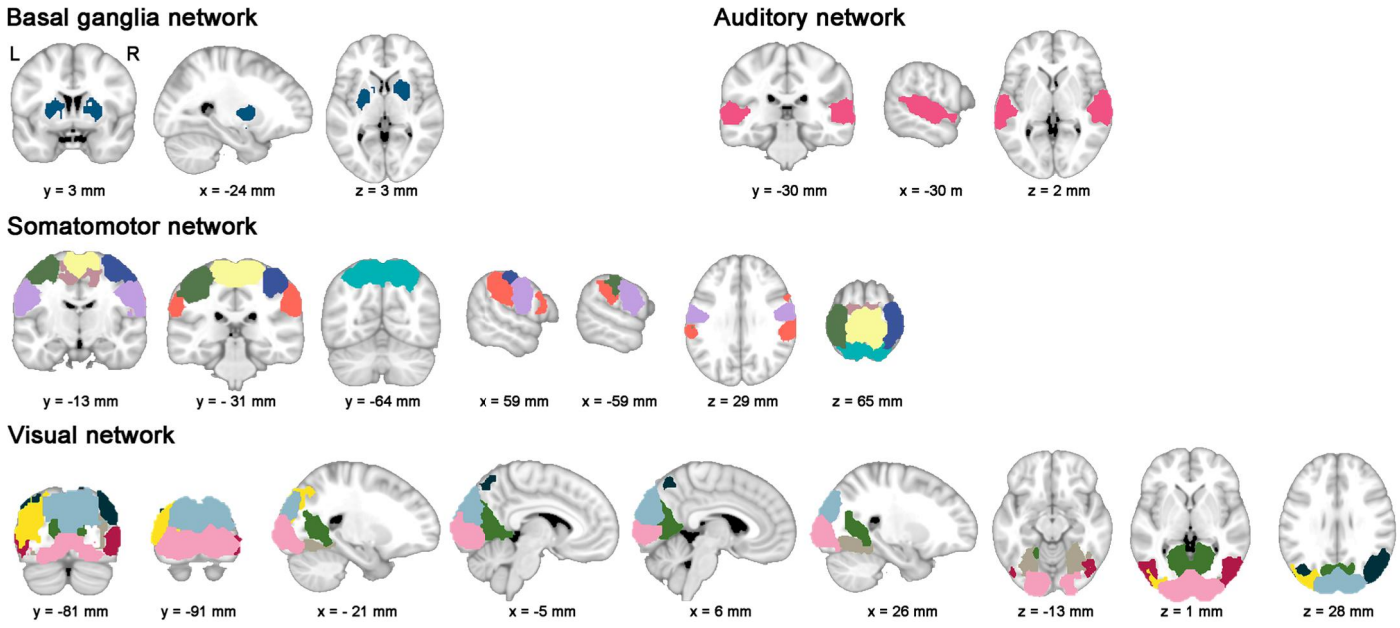

Figure 9. Functional networks composed of subsets of 31 independent components identified using one-sample t-test at family-wise error corrected $p < 0.01$, cluster size > 100 voxels. (Abbreviations: L = left, R = right)

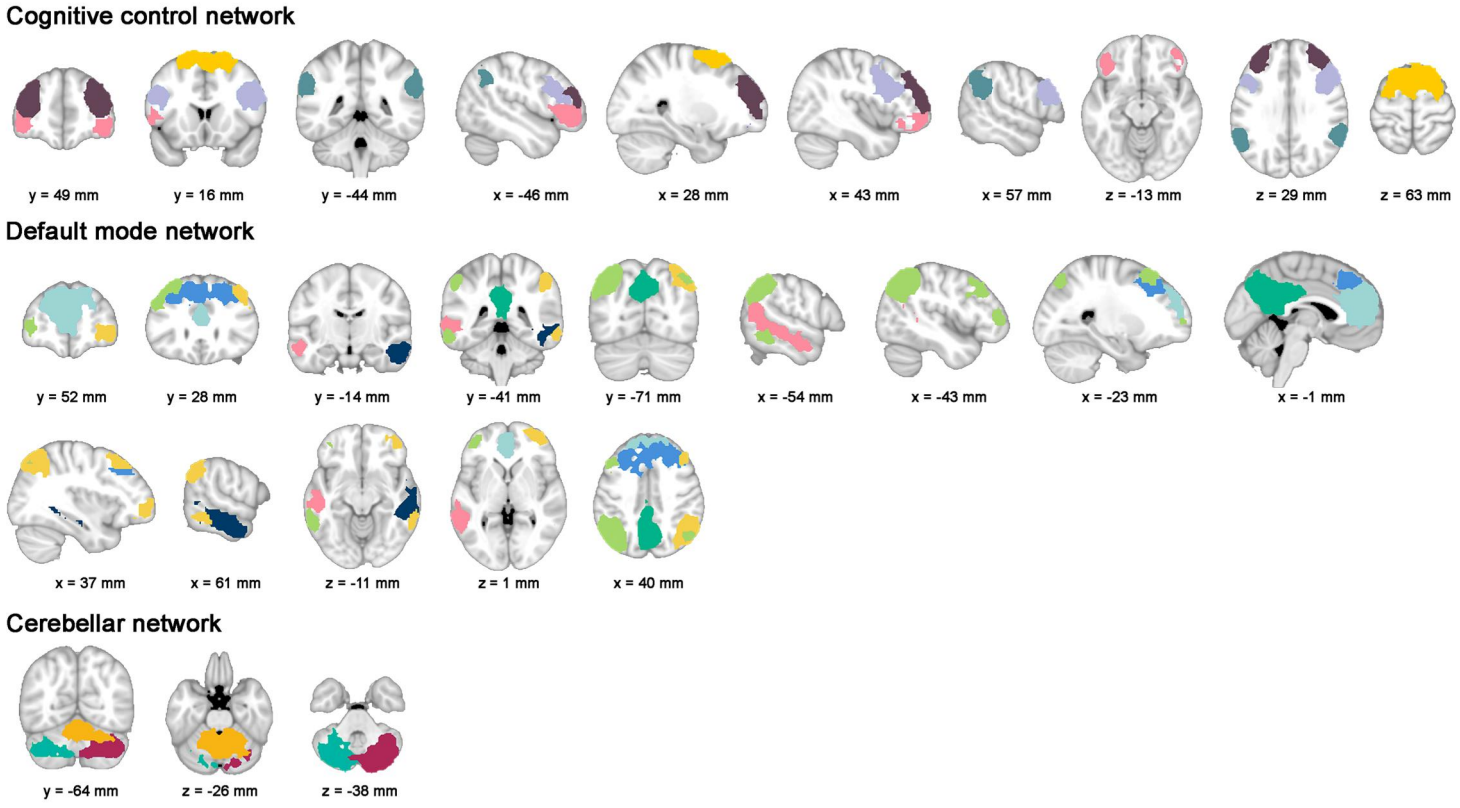

Figure 9 cont'd. Functional networks composed of subsets of 31 independent components identified using one-sample t-test at family-wise error corrected $p < 0.01$, cluster size > 100 voxels. (Abbreviations: L = left, R = right)

Table 7. Brain regions of independent components (IC) of intrinsic connectivity networks

	Brain region	k	T-value	x	y	z
Basal ganglia (BG) network						
● **IC 30**	Putamen, L	196	13.41	-24	3	3
	Putamen, R	273	12.31	21	6	-3
Auditory (AUD) network						
● **IC 33**	Superior temporal gyrus, R	1025	19.11	63	-21	3
	Superior temporal gyrus, R		15.22	57	-18	9
	Superior temporal gyrus, R		14.95	60	-33	9
	Superior temporal gyrus, L	745	13.22	-60	-18	3
	Superior temporal gyrus, L		12.37	-48	-24	3
	Superior temporal gyrus, L		11.71	-60	-30	9
Somatomotor (SM) network						
● **IC 02**	Postcentral gyrus, L	606	25.46	-57	-9	24
	Postcentral gyrus, L		21.57	-57	-6	33
	Postcentral gyrus, L		8.47	-57	-9	48
	Postcentral gyrus, R	743	22.65	54	-6	27
	Precentral gyrus, R		20.29	54	-9	39
	Postcentral gyrus, R		19.96	63	-3	33
● **IC 03**	Precentral gyrus, R	1302	21.36	42	-21	60
	Postcentral gyrus, R		21.10	42	-33	63
	Precentral gyrus, R		21.01	33	-15	69
● **IC 04**	Postcentral gyrus, L	1643	19.02	-45	-33	57
	Precentral gyrus, L		17.62	-39	-18	60
	Postcentral gyrus, L		16.62	-36	-36	48
● **IC 06**	Paracentral lobule, L	2027	20.41	0	-18	63
	Paracentral lobule, L		18.87	-3	-33	60
	Paracentral lobule, R		18.19	9	-36	69
● **IC 29**	Superior parietal gyrus, R	2545	18.55	30	-60	57
	Superior parietal gyrus, L		18.28	-18	-63	60
	Superior parietal gyrus, L		17.97	-21	-72	54
● **IC 32**	Supramarginal gyrus, R	980	17.57	63	-33	39
	Supramarginal gyrus, R		17.49	63	-24	36
	Supramarginal gyrus, R		15.04	60	-24	24
	Supramarginal gyrus, L	365	13.32	-63	-27	33
	Inferior parietal gyrus, L		9.40	-48	-42	54
	Inferior parietal gyrus, L		8.08	-42	-42	45
	Middle frontal gyrus, R	203	12.11	42	42	21
	Inferior frontal gyrus (triangular), R		9.89	48	39	6
	Middle frontal gyrus, R		6.78	33	51	27
	Inferior frontal gyrus (opercular), R	232	10.63	54	12	9
	Inferior frontal gyrus (opercular), R		10.56	48	12	15

	Inferior frontal gyrus (opercular), R		9.79	60	15	30
IC 39	Supplementary motor area, L	1090	15.11	-9	-9	51
	Supplementary motor area, R		11.86	3	-12	60
	Middle cingulate, R		11.74	15	-9	45
Visual (VIS) network						
IC 01	Middle occipital gyrus, L	2265	30.77	-24	-93	-3
	Middle occipital gyrus, L		26.31	-21	-102	0
	Calcarine gyrus, R		25.99	21	-99	0
IC 05	Superior occipital gyrus, R	1964	21.90	21	-90	24
	Cuneus, R		21.26	6	-90	24
	Cuneus, R		20.80	12	-87	42
IC 09	Calcarine gyrus, L	2600	23.86	-15	-66	6
	Calcarine gyrus, L		20.68	-3	-72	18
	Calcarine gyrus, L		20.35	-9	-66	15
IC 27	Middle occipital gyrus, L	1245	17.10	-33	-90	24
	Middle occipital gyrus, L		15.66	-24	-93	30
	Middle occipital gyrus, L		14.88	-39	-90	12
IC 40	Middle occipital gyrus, R	840	21.90	42	-78	33
	Middle temporal gyrus, R		13.96	54	-60	21
	Middle temporal gyrus, R		7.37	57	-48	6
	Middle occipital gyrus, L	375	18.15	-33	-78	36
	Angular gyrus, L		9.62	-54	-69	24
	Precuneus, R	200	10.57	6	-66	57
	Superior parietal gyrus, R		9.60	15	-75	54
	Precuneus, L		9.36	-6	-69	57
IC 49	Middle temporal gyrus, R	1040	23.05	54	-66	9
	Middle temporal gyrus, R		22.29	54	-72	3
	Inferior temporal gyrus, R		15.63	51	-72	-9
	Middle occipital gyrus, L	556	18.82	-45	-78	3
	Inferior occipital gyrus, L		14.02	-45	-78	-9
	Middle occipital gyrus, L		10.66	-36	-93	0
IC 50	Lingual gyrus, R	815	15.02	24	-57	-9
	Fusiform gyrus, R		14.48	27	-72	-6
	Fusiform gyrus, R		14.31	30	-57	-15
	Fusiform gyrus, L	397	13.45	-30	-69	-12
	Fusiform gyrus, L		9.83	-36	-63	-18
	Lingual gyrus, L		9.70	-21	-66	-12
Cognitive control (CC) network						
IC 12	Middle frontal gyrus, L	865	17.94	-36	48	15
	Superior frontal gyrus, L		14.25	-27	60	12
	Middle frontal gyrus, L		13.60	-36	42	30
	Middle frontal gyrus, R	785	14.67	39	39	33
	Superior frontal gyrus, R		13.60	33	57	15

	Middle frontal gyrus, R		13.44	42	51	12
IC 19	Superior frontal gyrus, L	756	16.58	-36	57	0
	Inferior frontal gyrus (triangular), L		15.88	-48	39	-3
	Inferior frontal gyrus (triangular), L		13.80	-39	36	0
	Inferior frontal gyrus (orbital), R	303	10.24	45	45	-12
	Orbitofrontal gyrus (anterior), R		9.93	39	51	-15
	Inferior frontal gyrus (triangular), R		9.90	48	39	-3
IC 28	Supplementary motor area, L	1518	19.92	-12	15	66
	Superior frontal gyrus, R		13.78	18	21	63
	Superior frontal gyrus, L		13.76	-24	21	60
IC 35	Supramarginal gyrus, L	531	22.38	-57	-51	30
	Middle temporal gyrus, L		8.05	-54	-66	18
	Inferior parietal gyrus, L		6.96	-42	-60	51
	Supramarginal gyrus, R	424	16.63	60	-48	36
	Angular gyrus, R		15.24	60	-54	27
	Supramarginal gyrus, R		12.34	54	-42	27
IC 45	Inferior frontal gyrus (triangular), R	860	16.71	48	21	27
	Inferior frontal gyrus (triangular), R		15.98	42	18	21
	Inferior frontal gyrus (opercular), R		15.63	54	21	33
	Inferior frontal gyrus (triangular), L	381	12.83	-48	21	27
	Inferior frontal gyrus (opercular), L		10.71	-45	12	27
	Inferior frontal gyrus (triangular), L		10.24	-51	33	18
Default mode (DM) network						
IC 08	Angular gyrus, L	1176	25.50	-42	-69	45
	Inferior parietal gyrus, L		22.96	-42	-60	51
	Inferior parietal gyrus, L		18.93	-45	-57	42
	Inferior frontal gyrus (triangular), L	208	12.63	-45	48	3
	Middle frontal gyrus, L		9.15	-39	45	-6
	Superior frontal gyrus, L		8.38	-18	57	6
	Middle frontal gyrus, L	515	12.58	-27	24	57
	Middle frontal gyrus, L		11.91	-36	24	51
	Middle frontal gyrus, L		10.68	-48	24	36
	Angular gyrus, R	188	12.24	48	-69	42
	Inferior parietal gyrus, R		8.35	48	-51	51
	Middle temporal gyrus, L	237	11.99	-60	-42	-12
	Inferior temporal gyrus, L		8.46	-54	-54	-12
	Inferior temporal gyrus, L		8.28	-63	-24	-18
IC 10	Superior frontal gyrus (medial), L	2036	24.57	-3	48	24
	Superior frontal gyrus (medial), L		22.97	3	51	30
	Superior frontal gyrus (medial), R		20.87	6	51	18
IC 16	Precuneus, L	1691	26.31	-3	-66	36
	Posterior cingulate, L		20.12	-3	-51	30
	Precuneus, L		17.89	-12	-63	30

	Angular gyrus, L	185	10.89	-45	-66	36
	Angular gyrus, L		10.31	-39	-75	42
IC 17	Angular gyrus, R	971	25.89	42	-66	51
	Inferior parietal gyrus, R		25.52	48	-57	48
	Inferior parietal gyrus, R		23.32	54	-57	42
	Middle frontal gyrus, R	340	13.06	42	48	-3
	Superior frontal gyrus, R		12.30	30	54	-6
	Middle frontal gyrus, R		11.39	33	54	3
	Middle frontal gyrus, R	303	12.12	36	21	45
	Middle frontal gyrus, R		11.80	39	18	54
	Middle frontal gyrus, R		11.21	39	30	42
	Inferior temporal gyrus, R	137	9.42	60	-54	-12
	Inferior temporal gyrus, R		8.84	63	-42	-12
	Middle temporal gyrus, R		8.17	66	-30	-15
IC 18	Superior frontal gyrus, L	1743	14.56	-15	36	51
	Superior frontal gyrus, R		13.15	18	36	48
	Middle frontal gyrus, L		13.14	-21	24	48
IC 34	Middle temporal gyrus, L	861	15.02	-54	-39	0
	Middle temporal gyrus, L		11.92	-63	-30	-6
	Middle temporal gyrus, L		11.27	-54	-63	18
IC 38	Inferior temporal gyrus, R	994	14.48	51	-18	-21
	Inferior temporal gyrus, R		11.83	57	0	-27
	Inferior temporal gyrus, R		11.44	57	-24	-24
Cerebellar (CB) network						
IC 11	Vermis	1320	22.71	3	-57	-27
	Cerebellum, R		16.34	21	-54	-30
	Cerebellum, R		15.53	9	-60	-21
IC 14	Cerebellum, R	1496	16.42	33	-84	-39
	Cerebellum, R		14.95	33	-63	-39
	Cerebellum, R		14.52	15	-84	-42
IC 26	Cerebellum, L	1309	13.00	-18	-81	-39
	Cerebellum, L		12.83	-36	-66	-39
	Cerebellum, L		12.61	-30	-81	-39

The coordinates are the peak activation in Montreal Neurological Institute space from one-sample t-test of independent component spatial maps of all subjects at family-wise error corrected *p*-value < 0.01 and cluster extent size (k) > 100 voxels. (Abbreviations: IC = independent component, L = left, R = right)

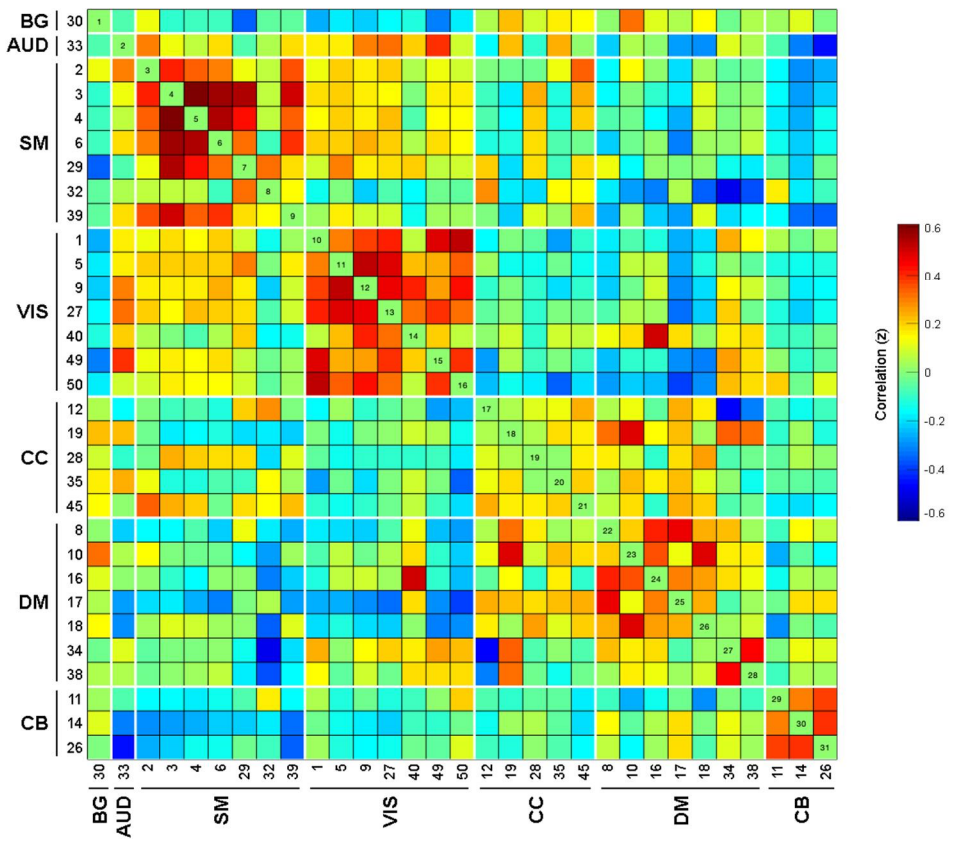

Figure 10. Averaged static functional connectivity matrix between independent components grouped into seven functional networks. The left and bottom of the matrix shows the index number of independent components. Warm color indicates positive functional connectivity, and cool color indicates negative functional connectivity. (Abbreviations: BG = basal ganglia, AUD = auditory, SM = somatomotor, VIS = visual, CC = cognitive control, DM = default mode, CB = cerebellar)

4.4.2 Dynamic functional connectivity states

Four functional connectivity state patterns were identified using *k*-means clustering analysis and elbow method (Figure 11). Figure 12 displays cluster centroids of each functional connectivity state, which are the median of the functional connectivity matrices assigned to the state. State 1 accounts for 43 % of all windows and resembles the pattern of the static functional connectivity matrix. It exhibits mostly sparse and positive functional connectivity within networks. State 2 is the second most frequent state, which shows stronger functional connectivity (both positive and negative) between networks than State 1. The degree of functional connectivity strengths within- and between-networks of State 2 appears to lie intermediate between those of State 1 and State 3. Positive functional connectivity between sensorimotor networks including AUD, SM, and VIS networks and positive DM network connectivity are notably observed. State 3 shows strong positive functional connectivity between SM, AUD, and VIS networks, and strong negative functional connectivity between SM, CC, and DM networks. Cerebellar functional connectivity is also heightened. State 4 is the least frequently reoccurring, and it is distinguished from the other states by a differential pattern of reduced functional connectivity of sensorimotor networks. SM network shows asynchronous activations with sensory networks as well as with CB network. Strong within-network couplings of CB network and more disintegrated couplings of DM network are also evident. Group-specific centroids of the states were calculated by averaging subject-specific centroids for subjects with finite correlations for each group (Figure 13). Similar patterns and frequencies of dynamic functional connectivity states were evident for each group.

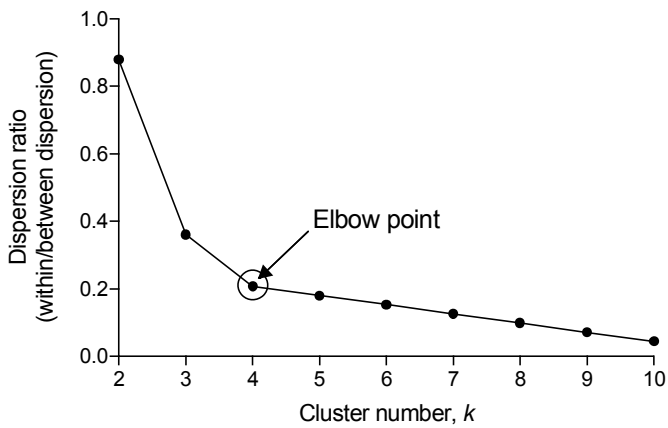

Figure 11. Elbow plot for *k*-means clustering method. Dispersion ratio is the ratio of the sum of within-cluster distance to the sum of between-cluster distance, at each *k* value. The optimal number of clusters indicated by elbow point in the plot is determined to be four.

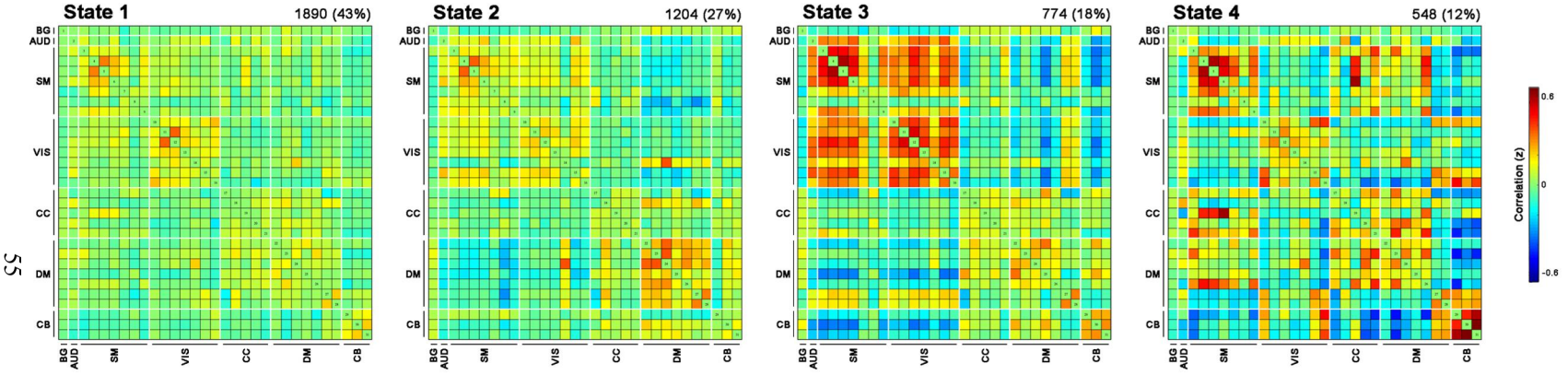

Figure 12. Cluster centroids for four functional connectivity states. The total number of occurrences and percentage of each state during the scan time are displayed on the right above the connectivity matrix. Warm color indicates positive functional connectivity, and cool color indicates negative functional connectivity. (Abbreviations: BG = basal ganglia, AUD = auditory, SM = somatomotor, VIS = visual, CC = cognitive control, DM = default mode, CB = cerebellar)

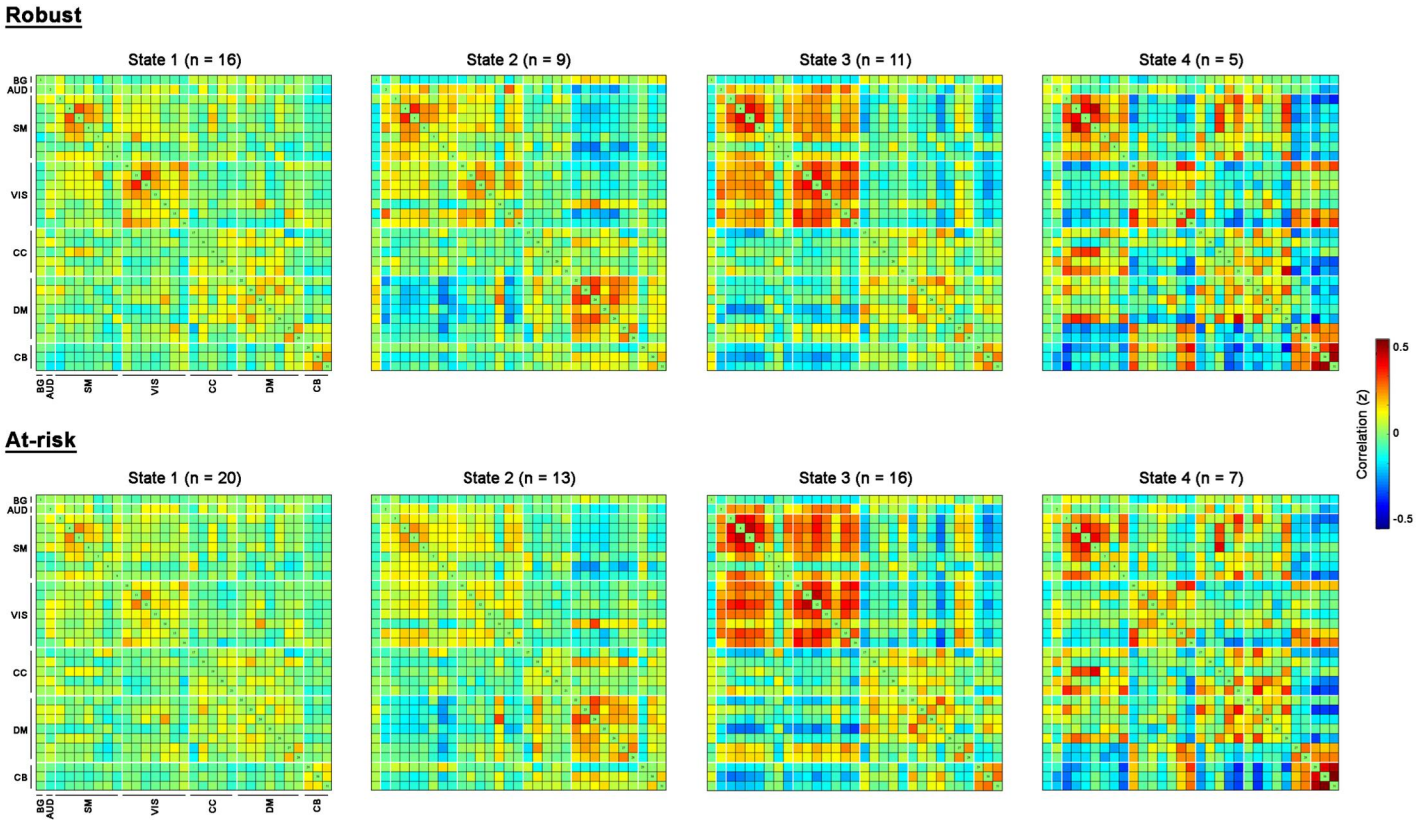

Figure 13. Group-specific cluster centroids of the four functional connectivity states. The number of subjects with finite correlations is displayed above the connectivity matrix of each state. Warm color indicates positive functional connectivity, and cool color indicates negative functional connectivity. (Abbreviations: BG = basal ganglia, AUD = auditory, SM = somatomotor, VIS = visual, CC = cognitive control, DM = default mode, CB = cerebellar)

4.4.3 Validation results of dynamic functional connectivity states

Reproducibility analyses confirmed the robustness of the *k*-means clustering analysis results. The results demonstrated that the functional connectivity patterns and relative reoccurrences of the states persisted for different numbers of *k* (Figure 14). Furthermore, the additional cluster centroids observed when using a higher value of *k*, resembled the patterns of centroids at $k = 4$, which supports the optimal value of *k* used in the current results. For bootstrap samples, the occurrences of dynamic functional connectivity states were similar with the original data. The number of occurrences of State 1 and State 2 for original data lied well within the 95 % confidence intervals of the average number of occurrences for bootstrap samples (Table 8, Figure 15). The functional connectivity patterns of states for bootstrap datasets highly resembled the pattern for original dataset (Figure 16).

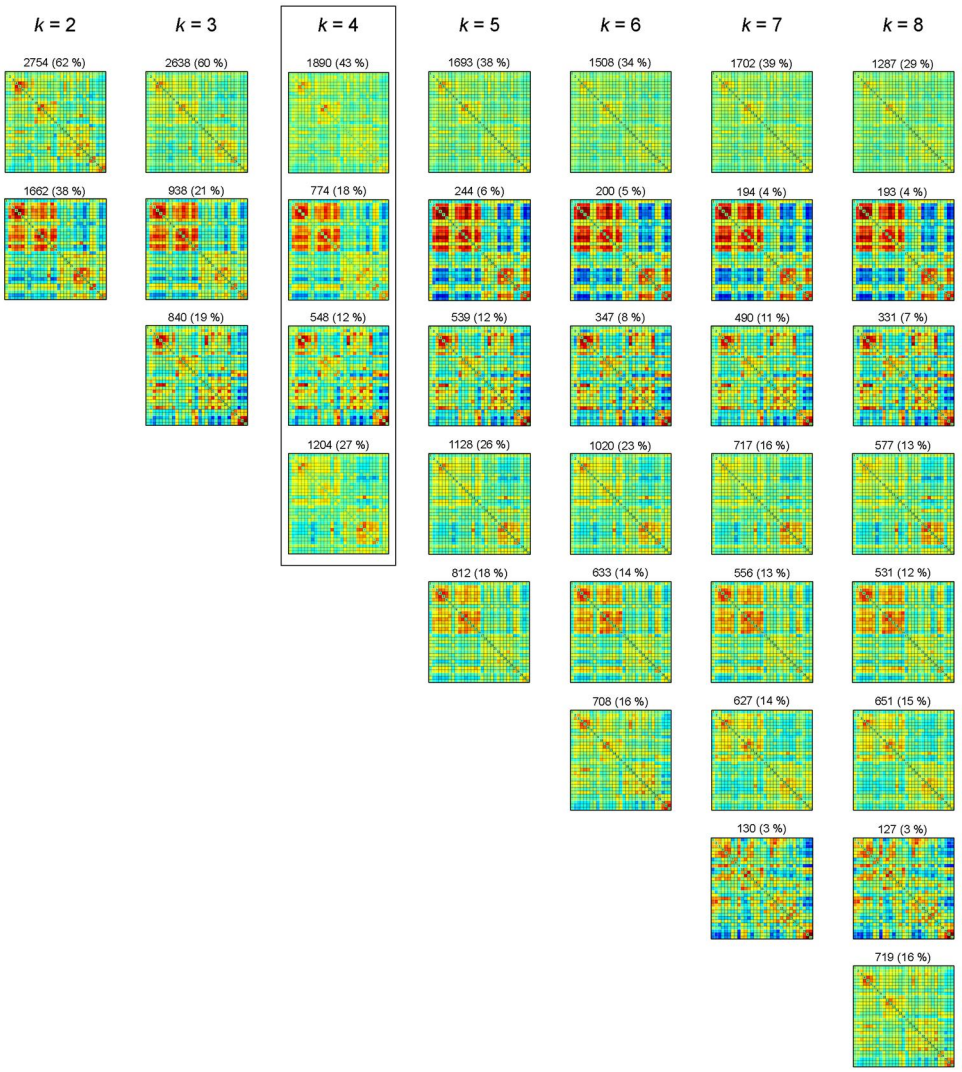

Figure 14. Cluster centroids for a range of *k*. The number of occurrences and percentages are displayed above the cluster centroid. The rectangle highlights the optimal number of clusters which are used in the further analysis.

Table 8. Occurrences of dynamic functional connectivity states for original and bootstrap resampled datasets

	Original dataset		Bootstrap resampled datasets	
	Total number of occurrences	**Occurrences in %**	**Total number of occurrences (95 % C.I.)**	**Occurrences in %**
State 1	1890	42.8	1903 (1846 – 1960)	43.1
State 2	1204	27.3	1112 (1045 – 1178)	25.2
State 3	774	17.5	690 (647 – 734)	15.6
State 4	548	12.4	710 (670 – 750)	16.1

(Abbreviations: C.I. = confidence interval)

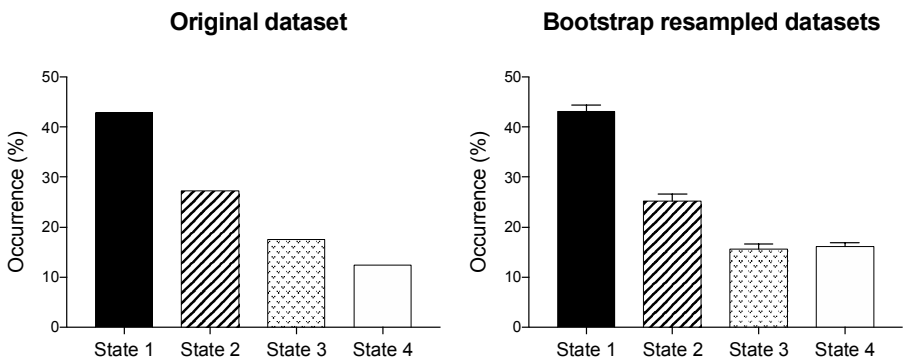

Figure 15. Occurrences of dynamic functional connectivity states for original (left) and bootstrap resampled (right) datasets.

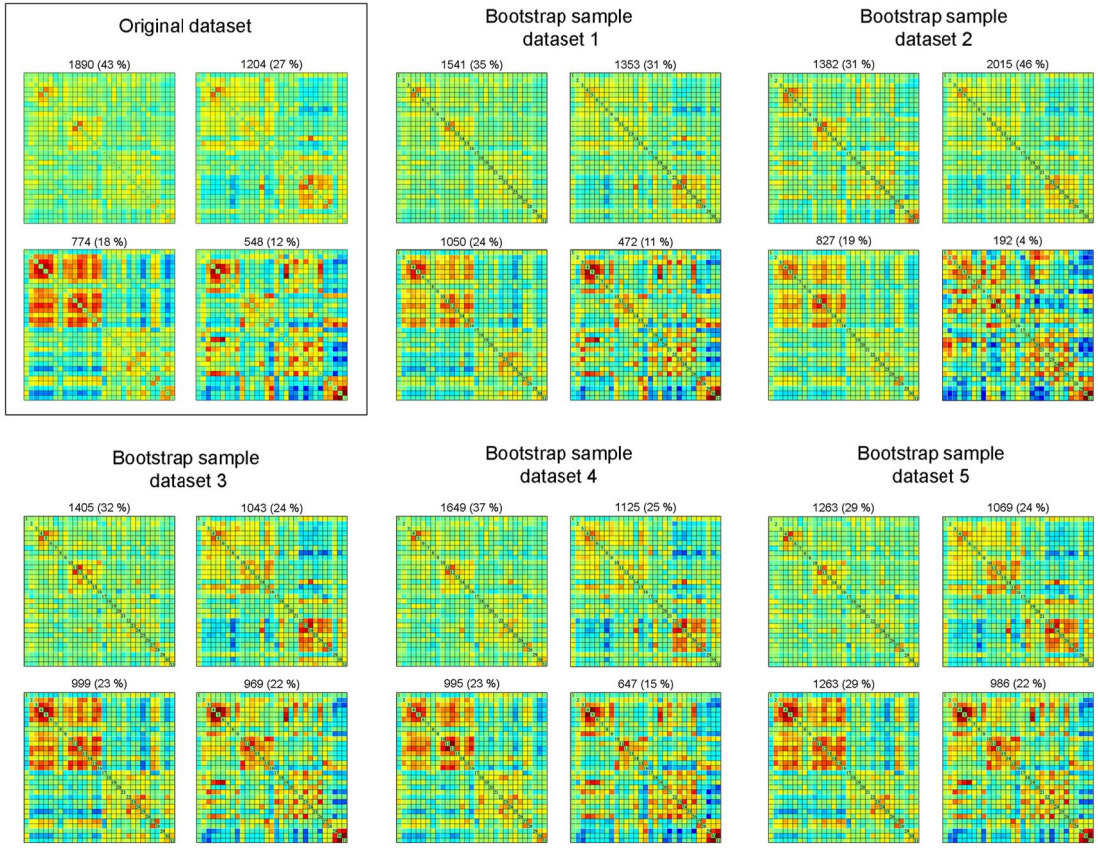

Figure 16. Cluster centroids for five representative bootstrap resampled datasets. The rectangle highlights the cluster centroids for original dataset. Each bootstrap sample consisted of 46 subject data with replacement, and k-means clustering algorithm was applied with 500 iterations to each dataset. The number and percentage of occurrences are displayed above each cluster centroid.

4.4.4 Temporal properties of dynamic functional connectivity states

Table 9 and Figure 17 summarize the temporal properties of the functional connectivity states. The number of state transitions was 3.65 (± 2.81) and 3.77 (± 2.64) in robust group and at-risk group, respectively, and the group difference failed to reach a statistical significance. The fractional windows of State 1 and State 3 are 13 % lower and 11 % higher in at-risk group than in robust group, however, the changes in fractional windows in at-risk group were not statistically significant. Similarly, the mean dwell time of State 1 in at-risk group is shorter (mean: 18.84 ± 24.92 windows) compared to robust group (mean: 31.4 ± 33.99 windows), whereas the mean dwell time of State 3 is relatively longer in at-risk group (mean: 14.61 ± 25.06 windows) than in robust group (mean: 6.66 ± 6.58 windows). Nevertheless, the group difference in the mean dwell time did not reach the statistical significance.

In addition to the temporal properties of the connectivity states, the occurrence of states as a function of time was examined (Figure 18). It is evident that State 1 appears throughout the scan time in a large number of subjects in each group. The expression of State 1 changes with the changes in the expression of State 2 and State 3, meaning that the expression of State 2 and State 3 increases when State 1 is expressed less. In robust group, the number of occurrences of State 2 slowly drops as the scan progress, whereas it remains relatively high until the end of the scan time in at-risk group. One striking feature in the occurrence of states in at-risk group is that State 3 is expressed in a relatively large number of subjects, and it persists throughout the scan time. State 4 is increasingly more frequently appearing over time similarly in both groups.

Table 9. Temporal properties of dynamic functional connectivity states

		Robust (n = 20)	At-risk (n = 26)	*p*-value[¶]
Number of transitions		3.65 (2.81)	3.77 (2.64)	0.881
Fractional windows	State 1	0.50 (0.36)	0.37 (0.43)	0.218
	State 2	0.25 (0.34)	0.29 (0.35)	0.774
	State 3	0.11 (0.15)	0.22 (0.29)	0.355
	State 4	0.13 (0.30)	0.12 (0.24)	0.804
Mean dwell time	State 1	31.35 (33.99)	18.84 (24.92)	0.444
	State 2	12.01 (20.07)	14.47 (21.32)	0.720
	State 3	6.66 (33.99)	14.61 (25.06)	0.411
	State 4	8.35 (21.90)	7.08 (19.24)	0.782

Values are means (standard deviations)
[¶] Using chi-square test

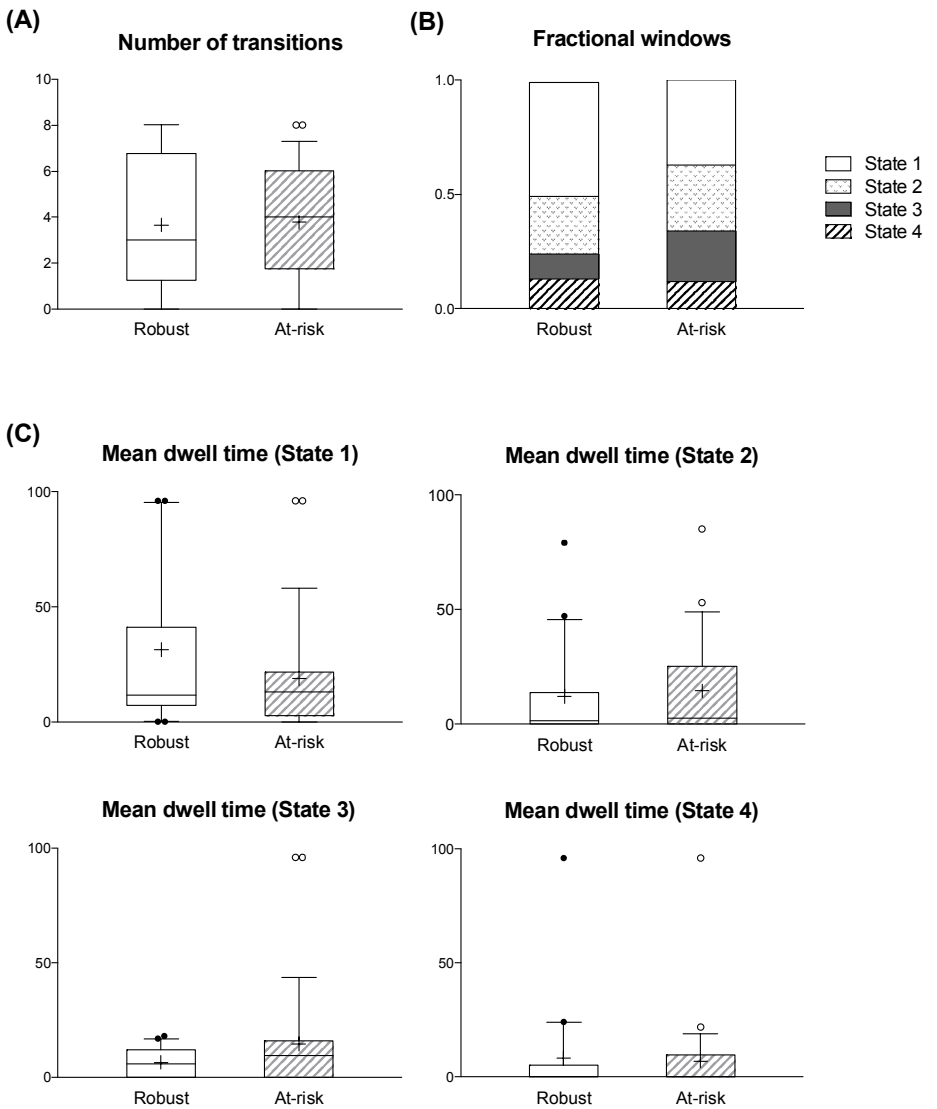

Figure 17. Box plots of (A) number of transitions, (B) fractional windows, and (C) mean dwell time of dynamic functional connectivity states in robust and at-risk group. Whiskers show 10 - 90 percentiles, and (+) sign shows a mean.

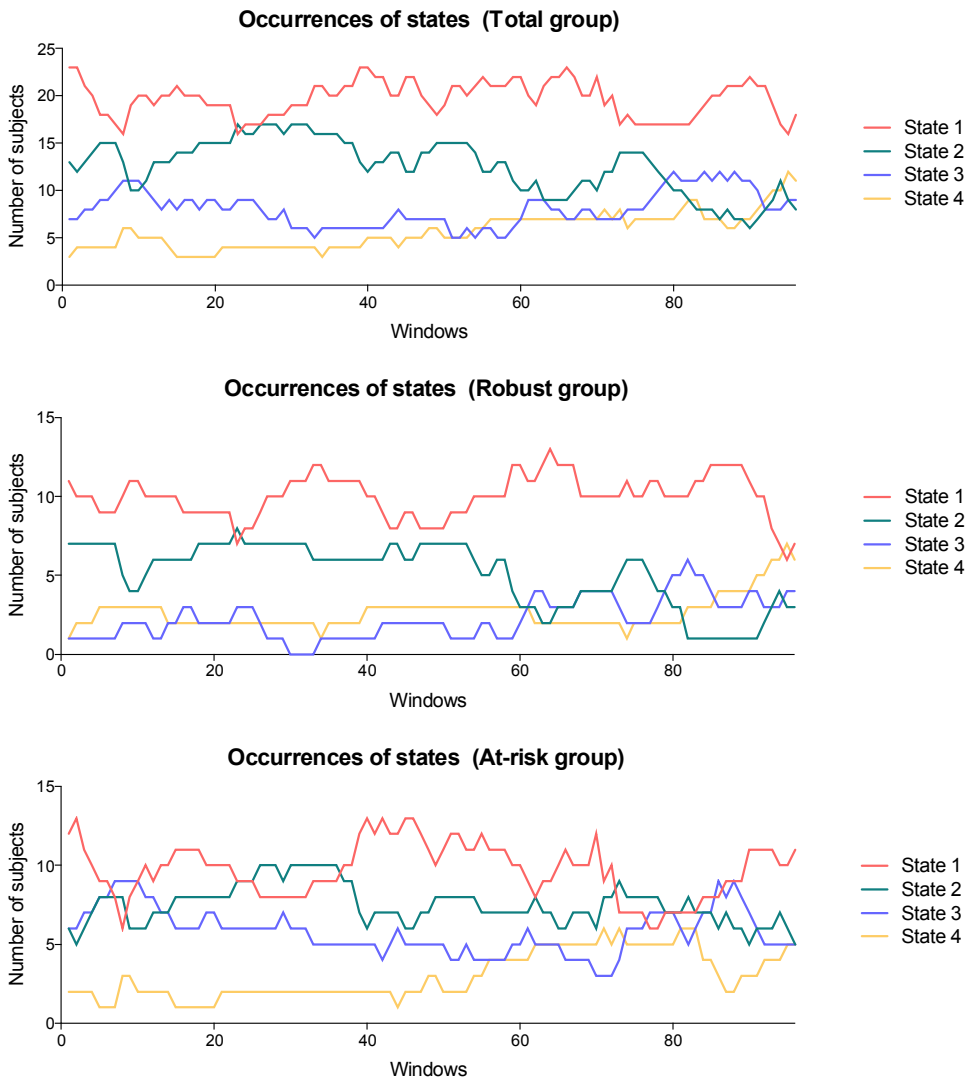

Figure 18. Occurrences of dynamic functional connectivity states as a function of time.

4.4.5 Relationships between dynamic functional connectivity measures and physical and cognitive performances

As displayed in Table 10 and Figure 19, multiple regression analyses revealed that the reductions in the fractional windows and mean dwell time of State 1 correlated with decreasing handgrip strength (β = 0.395 and 0.450, p = 0.007 and 0.001, respectively), meaning that individuals with muscle weakness were less likely to enter and stay long in State 1. The fractional windows of State 2 negatively correlated with MMSE-K (β = -0.393, p = 0.008), reflecting that patients with higher reoccurrence of State 2 during resting state display poorer MMSE-K scores. Increasing mean dwell time in State 2 also correlated with lower MMSE-K score (β = -0.469, p = 0.001).

Table 10. Multiple regression analysis results for physical and cognitive performances associated with temporal properties of dynamic functional connectivity states

			Adj. R^2	β	*p*	VIF
State 1 fractional windows						
Physical performance	Single (enter)	Grip strength *	0.139	0.397	0.006	
		Timed walk	0.010	-0.181	0.235	
		Physical activity *	0.101	0.318	0.031	
		Weight loss	-0.022	0.020	0.894	
		Exhaustion	-0.010	-0.112	0.460	
	Multiple (stepwise)	Grip strength	0.137	0.395	0.007	1.000
		Timed walk		-0.050	0.744	1.137
		Physical activity		0.206	0.162	1.090
		Weight loss		0.015	0.914	1.000
		Exhaustion		-0.030	0.839	1.045
Cognitive performance	Single (enter)	Memory	0.030	0.227	0.130	
		Visuospatial	-0.017	0.072	0.635	
		Executive	0.020	0.205	0.172	
		Language	-0.014	0.092	0.554	
		MMSE-K	0.024	0.214	0.152	
	Multiple (stepwise)	none				
State 1 mean dwell time						
Physical performance	Single (enter)	Grip strength *	0.168	0.432	0.003	
		Timed walk	0.021	-0.209	0.168	
		Physical activity *	0.090	0.332	0.024	
		Weight loss	-0.023	0.002	0.988	
		Exhaustion	-0.001	-0.147	0.329	
	Multiple (stepwise)	Grip strength	0.166	0.430	0.003	1.000
		Timed walk		-0.068	0.648	1.137
		Physical activity		0.216	0.135	1.090
		Weight loss		-0.004	0.975	1.000
		Exhaustion		-0.059	0.678	1.045
Cognitive performance	Single (enter)	Memory	0.055	0.276	0.064	
		Visuospatial	0.030	0.228	0.128	
		Executive	-0.005	0.131	0.385	
		Language	0.037	0.241	0.107	
		MMSE-K	0.008	0.175	0.246	
	Multiple (stepwise)	none				
State 2 fractional windows						
Physical performance	Single (enter)	Grip strength	0.014	-0.189	0.207	
		Timed walk	-0.013	0.099	0.520	
		Physical activity	-0.017	-0.077	0.610	
		Weight loss	-0.017	-0.078	0.608	

		Exhaustion	-0.015	-0.088	0.559	
	Multiple (stepwise)	none				
Cognitive performance	Single (enter)	Memory	0.047	-0.261	0.079	
		Visuospatial	0.025	-0.217	0.147	
		Executive	0.043	-0.254	0.089	
		Language	-0.014	-0.094	0.536	
		MMSE-K *	0.166	-0.430	0.003	
	Multiple (stepwise)	MMSE-K *	0.166	-0.430	0.003	1.000
		Memory		-0.057	0.726	1.354
		Visuospatial		-0.124	0.383	1.057
		Executive		-0.129	0.375	1.116
		Language		-0.046	0.741	1.013
State 2 mean dwell time						
Physical performance	Single (enter)	Grip strength	-0.003	-0.141	0.352	
		Timed walk	0.008	0.174	0.253	
		Physical activity	-0.021	-0.035	0.816	
		Weight loss	-0.023	0.001	0.992	
		Exhaustion	-0.015	-0.086	0.568	
	Multiple (stepwise)	none				
Cognitive performance	Single (enter)	Memory	-0.003	-0.140	0.355	
		Visuospatial	0.008	-0.173	0.250	
		Executive	0.062	-0.287	0.053	
		Language	0.014	-0.189	0.209	
		MMSE-K *	0.211	-0.478	0.001	
	Multiple (stepwise)	MMSE-K *	0.211	-0.478	0.001	1.000
		Memory		0.142	0.363	1.354
		Visuospatial		-0.065	0.638	1.057
		Executive		-0.149	0.293	1.116
		Language		-0.137	0.310	1.013

Asterisks indicate significant results at p-value < 0.05. (Abbreviations: MMSE-K = Korean version of Mini-Mental State Examination, Adj. R^2 = adjusted R^2, VIF = variance inflation factor)

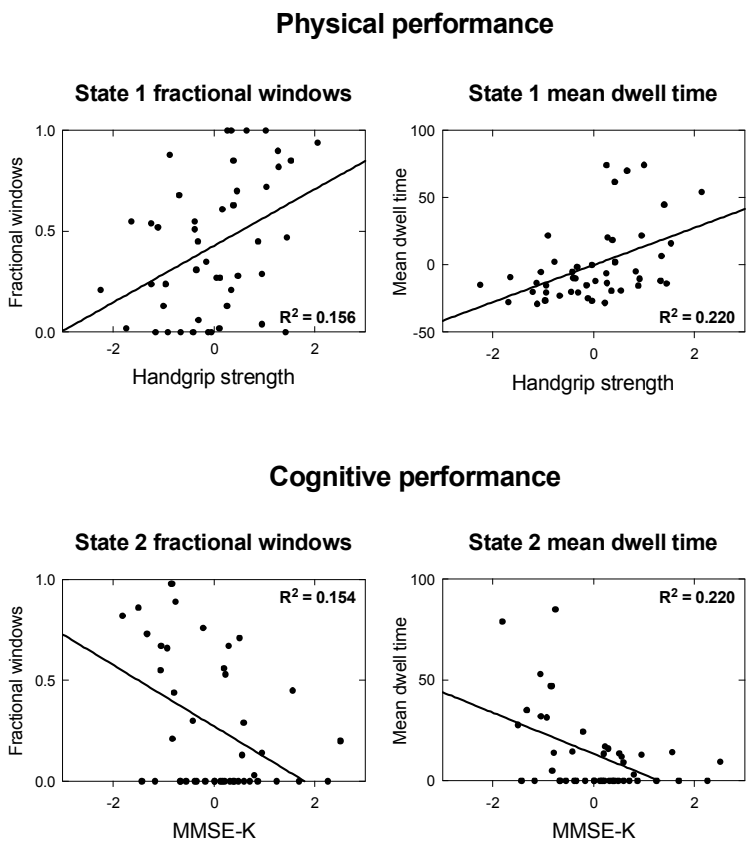

Figure 19. Plots of significant correlations between temporal properties of dynamic functional connectivity states and physical (above) and cognitive (below) performances. (Abbreviations: MMSE-K = Korean version of Mini-Mental State Examination)

4.4.6 Functional connectivity strengths in states

The functional connectivity strengths between independent network components for each state were compared between robust and at-risk groups, and the results in Figure 20 shows that the functional connectivity strengths between sensorimotor networks and cognitive networks were altered in at-risk group. In State 2, the functional connectivity between SM and CC networks was decreased, while functional connectivity the between VIS and DM networks was enhanced in at-risk group compared to robust group. Within CC network, the functional connection was also abnormally elevated in State 3 in at-risk group.

Relationships between functional connectivity strength changes between the network components with frailty phenotype measures and cognitive functions were also explored. However, the functional connectivity changes did not show any significant associations.

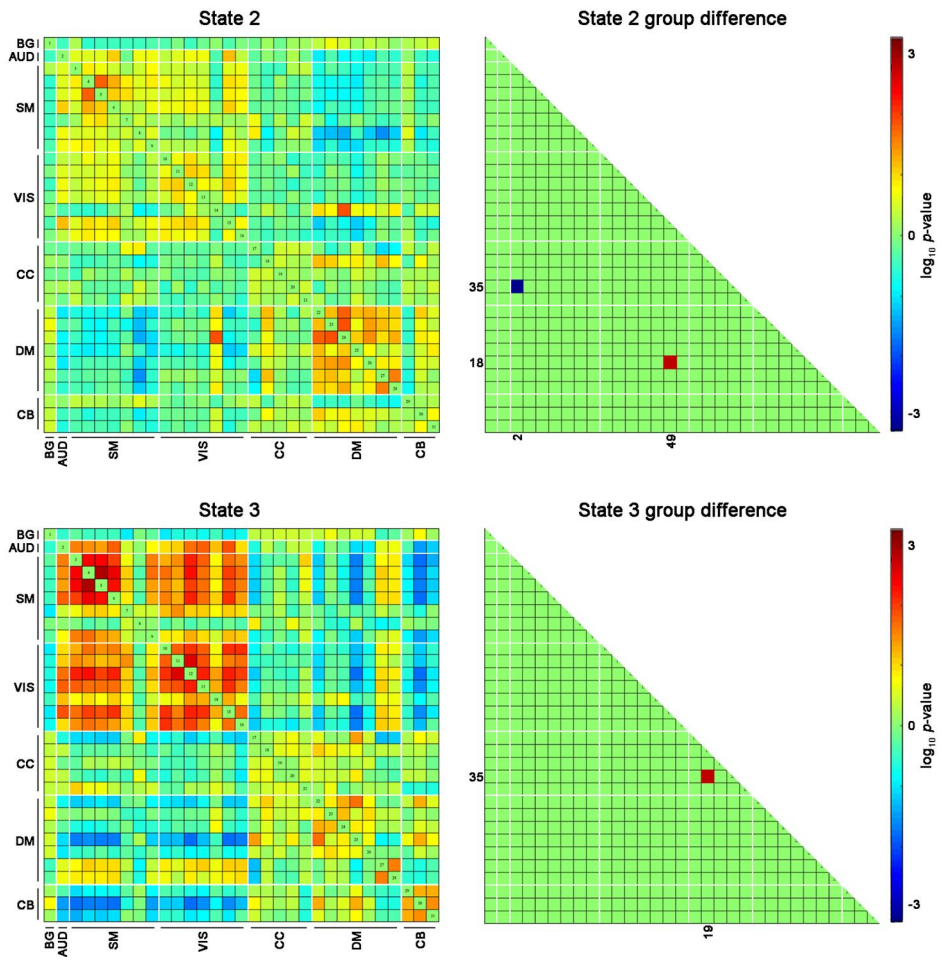

Figure 20. Changes in functional connectivity strengths between independent components in State 2 and State 3. Warm color indicates increased functional connectivity strength in at-risk group compared to robust group, and cool color indicates decreased functional connectivity strength. (Abbreviations: BG = basal ganglia, AUD = auditory, SM = somatomotor, VIS = visual, CC = cognitive control, DM = default mode, CB = cerebellar)

4.4.7 Dynamic changes of global and local network efficiency

The variability of network efficiency metrices over time was obtained by calculating interquartile range of the AUC values for each subject (Figure 21). Both global and local efficiency did not reach the statistical significance in group differences of the variability (Figure 22), although the variability in global efficiency had a tendency to be higher in at-risk group (p = 0.093, Mann-Whitney U test).

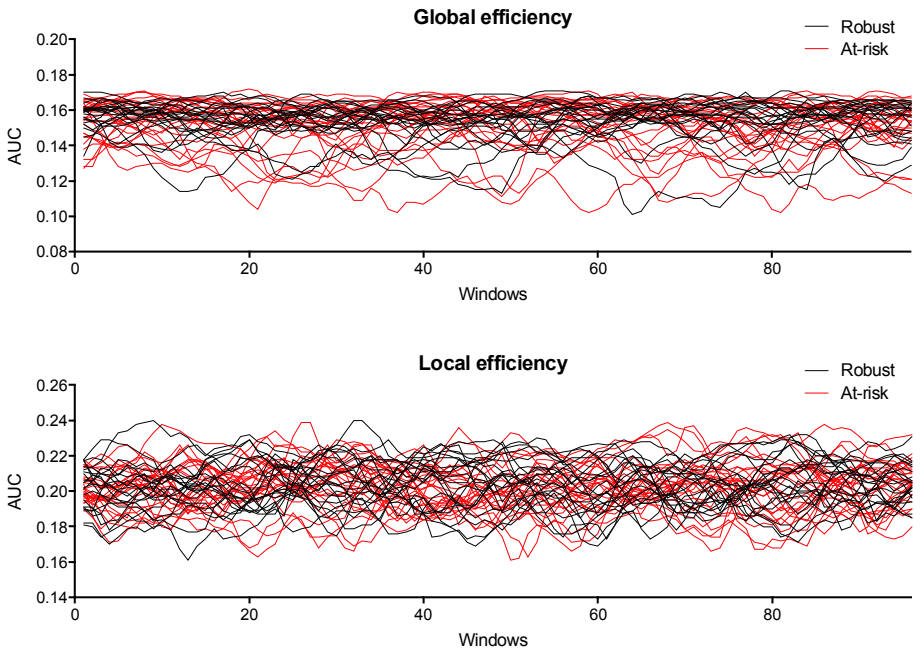

Figure 21. Dynamic changes in global efficiency (above) and local efficiency (below) of brain networks during the scan time. Black line indicates changes in robust group, and red line indicates changes in at-risk group. (Abbreviations: AUC = area under curve)

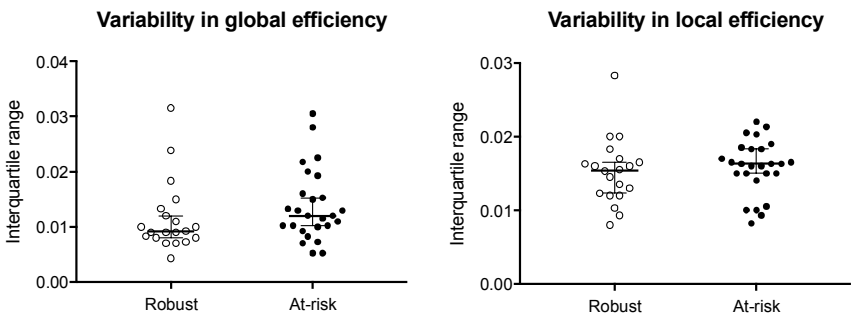

Figure 22. Comparisons of temporal variability of global efficiency (left) and local efficiency (right) between robust group and at-risk group.

Chapter 5. Discussion

5.1 Metabolic and functional abnormalities in cognitive frailty

The first part of the study was to explore alterations in metabolic and functional activities in patients with MCI with and without physical frailty. [^{18}F]FDG PET results showed that glucose metabolism was reduced in bilateral superior parietal cortex, right middle frontal cortex, and anterior cingulate in at-risk group. The reduced glucose metabolism in left superior parietal cortex was associated with weaker handgrip strength as well as with poorer performance in executive function. Regional synchronizations of functional activity measured by ReHo indicated reductions in bilateral caudate, right superior temporal cortex, right superior frontal cortex, and left cerebellum in at-risk group compared to robust group. Increased ReHo was also found in right precuneus and left cerebellum. The reduced ReHo in caudate was correlated with weaker handgrip strength and slowing of gait speed and also with language dysfunction. The reduction of ReHo in right superior temporal cortex was correlated with weakening of handgrip strength and a low level of physical activity, and it was also associated with a poorer performance in visuospatial function. Abnormally increased ReHo in right precuneus in at-risk group was associated with weak handgrip strength and memory function.

Our neuroimaging study demonstrated hypometabolism in parietal cortex, frontal cortex, and cingulate in patients with cognitive frailty, which is known as the hallmark of AD. The pattern of cortical metabolic changes in parieto-temporal, frontal, and cingulate areas has been useful to predict the conversion to AD in early stages and to distinguish AD from other neurodegenerative diseases (Mosconi,

2005). Despite no distinguishing cognitive impairments in at-risk individuals compared to robust group, our results indicate the expression of AD-related metabolic pattern in the presence of physical frailty. The metabolic abnormality in superior parietal cortex observed in at-risk individuals was clearly associated with physical disturbances as well as with cognitive dysfunctions. Posterior parietal cortex is known to be primarily involved in visuospatial attention, visually guided motor planning, and spatial representations in visuospatial tasks (Ghanavati, Salehinejad, Nejati, & Nitsche, 2019; Gurd et al., 2002; Kimberg, Aguirre, & D'Esposito, 2000; Sohn, Ursu, Anderson, Stenger, & Carter, 2000). Beyond visuospatial processing, the region is also implicated in working memory which underlies verbal fluency tasks (Gurd et al., 2002; Koenigs, Barbey, Postle, & Grafman, 2009; Sohn et al., 2000). Thereby, our results indicate that when accompanying physical weakness in MCI, the parietal cortex is significantly affected, and it may lead to exacerbation of cognitive decline in executive functions. Although no correlations between hypometabolism in frontal regions and anterior cingulate with physical performances in MCI were observed, the findings still signify that frontal and cingulate regions which are the core regions of high-order cognitive functions are considerably compromised in at-risk individuals, and it can be speculated that hypometabolism in frontal and anterior cingulate regions that are implicated in various cognitive functioning may lead to the emergence of related cognitive deficits at a faster rate in cognitive frailty.

Local synchronizations were noticeably decreased in caudate, right superior temporal cortex, and right frontal cortex in at-risk group. The functional changes in caudate was associated with handgrip weakness, slowness as well as with language dysfunction. Similar to our results, Chen et al. (2015) reported gray

matter atrophy in bilateral caudate in associations with physical weakness in older adults. Caudate controls the initiation and execution of voluntary motor activity, and its abnormal functional activity may be related to physical impairments that involve voluntary movements such as hand-gripping and walking. The functional activity of the region was also associated with performance in language. According to literature, caudate plays a role as a center for language control and participates to regulate articulation and comprehension of words and speech (Crinion et al., 2006). Furthermore, the region is functionally and anatomically connected with frontal areas, which implies that the structure is important for cognitive processes during language tasks, and damage to this area gives rise to language processing deficits (Gil Robles, Gatignol, Capelle, Mitchell, & Duffau, 2005; Gronholm, Roll, Horne, Sundgren, & Lindgren, 2016; Hillis et al., 2004). Abnormal functional activity in superior temporal cortex was evident in at-risk group and was linked to weak handgrip strength and low physical activity. Even though it is yet unsettled, the role of superior temporal cortex has been suggested in execution and observation of action (Kilintari, Raos, & Savaki, 2014), which helps explain our findings. The temporal region, which corresponds to Brodmann area 38 is one of the earliest regions affected in AD pathogenesis (Arnold, Hyman, Flory, Damasio, & Van Hoesen, 1991; Ding, Van Hoesen, Cassell, & Poremba, 2009), and is part of functional circuits involved in many higher brain functions such as memory, visual processing and language (Ardila, Bernal, & Rosselli, 2014; Ding et al., 2009). In line with this, the functional changes in superior temporal cortex has been associated with performance in visuospatial tests in our cohorts. Interestingly, right precuneus was abnormally highly synchronized in at-risk group, and positively correlated with memory function. As described above, the posterior cortex is

closely linked to various cognitive processes including memory (Cavanna & Trimble, 2006), and the elevation of functional synchronization in precuneus may reflect initial compensatory response prior to significant memory dysfunction in MCI. In short, we observed that in cognitive frailty, the metabolic and functional activity in several brain regions including parietal cortex, temporal cortex, and caudate, where are the regions that are primarily affected in early stages of AD, were significantly reduced, and the alterations were also relevant to cognitive decline.

Several neuroimaging studies have been conducted to investigate brain structural changes in associations with frailty components, and the results agreed that brain volume or integrity reductions are found in phenotypes of frailty (Camicioli, Moore, Sexton, Howieson, & Kaye, 1999; Rosano et al., 2010). For example, frail subjects showed increased ventricular size and increased white matter abnormalities (Newman et al., 2001; Rosano et al., 2005), and diffuse brain atrophy was associated with slowing of gait speed (Carmelli et al., 2000; Rosano et al., 2010). Gray matter volume reductions in dorsolateral prefrontal regions, basal ganglia, superior posterior parietal cortex, and cerebellum were also reported in association with slow gait speed (Rosano et al., 2007). Consistent to the previous findings, we also observed hypometabolism in bilateral superior parietal cortex, and functional alterations in caudate and superior temporal cortex, which were linked to physical impairments in cognitive frailty. Furthermore, the regional changes were also associated with cognitive functions including executive, visuospatial, and language functions.

As described previously, frailty and dementia are thought to share common neuropathological mechanisms, and it has been established that frailty is directly

influenced by AD pathology which leads to cognitive impairments (Buchman et al., 2008; Panza et al., 2011; Robertson et al., 2013; Schneider et al., 2006). In frailty without dementia, neurofibrillary tangles affected gait disturbances and eventually lead to development of dementia of AD. Moreover, a growing body of neuroimaging evidence revealed that amyloid-β accumulation in brain was associated with increasing frailty in older adults (Maltais et al., 2019; Yoon et al., 2018). In line with this, our findings support that significant functional abnormalities in brain regions that are specifically affected in AD dementia. Along with AD pathology, several other risk factors such as cardiovascular factors and aging-related biological parameters that are known to contribute to the development of frailty and dementia may also play a crucial role in the relationship between frailty and cognitive impairments (Langlois et al., 2012; Panza et al., 2018; Patrick, Gaskovski, & Rexroth, 2002; Ruan et al., 2015).

To sum up, our findings revealed that parietal, temporal and frontal cortex are mainly affected by handgrip strength, gait speed, and physical activity, and are closely linked to cognitive deteriorations in MCI.

5.2 Alterations of dynamic functional connectivity states in cognitive frailty

The second part of the study was to investigate alterations in dynamic functional connectivity patterns in MCI with and without physical frailty. The current study indicated that four functional connectivity patterns were identified in patients with MCI, and the temporal features of the connectivity states showed relationships with phenotypes of physical frailty as well as with cognitive function. The most frequently reoccurring State 1 displayed within-network connections with relatively weak between-network connections, while less frequently reoccurring

State 2 and State 3 exhibited stronger inter- and intra-connected networks in both positive and negative fashions. Despite no significant group differences found in the temporal properties of the states, it was detected that weaker handgrip strength was significantly correlated with the less reoccurrence and shorter mean dwell time of within-network State 1. On the other hand, the expression and mean dwell time of State 2 were elevated as MMSE-K score declined in MCI.

Our observations confirmed that resting state networks are vulnerable in pathological conditions as well as in normal aging. Formerly, there has been consistent evidence that the functional connectivity within brain network systems is compromised, paralleled by a relative increase in between-network interactions in healthy aging and in neurodegenerative diseases (Chan, Park, Savalia, Petersen, & Wig, 2014; Elman et al., 2016; Kim et al., 2017). The weaker within-network functional connectivity is interpreted as a decline of functional segregation or functional specificity with which neural networks mediate specialized processing roles (Chan et al., 2014; Sporns, 2013). Meanwhile, between-network interactions increase with continual aging, which may be perceived as adaptive responses to age-related alterations and beneficial effects to an individual. Rather, the abnormally increased interactions across distinct systems blur the functional specificity and diminish within-network communications, leading to negative outcomes on cognitive function (Chan et al., 2014). Comparatively, in at-risk individuals the expression of within-network State 1 was dropped by 13 %, while the expression of between-network State 2 and State 3 was risen by approximately the same amount. Furthermore, the reduced functional segregation was correlated with physical weakness and cognitive decline. Our results clearly characterize the

trend reported in aging processes and are suggestive of accelerated changes in MCI with physical frailty.

Intensive studies have demonstrated that within neural networks are pathologically disconnected in MCI and dementia (Andrews-Hanna et al., 2007; Chen et al., 2017; Seeley, Crawford, Zhou, Miller, & Greicius, 2009), and the disruption of large-scale neural networks was clearly associated with cognitive dysfunction across a range of domains. Previous dynamic functional connectivity studies revealed reduced dwell time in hypo-connected state in association with MCI in Parkinson's disease patients, implying that the temporal properties of functional networks mirror cognitive performance (Diez-Cirarda et al., 2018). Also, the clinical motor symptom severity of Parkinson's disease was also correlated with the alteration in dynamic functional connectivity states (Kim et al., 2017).

In State 1, positive functional connections mainly can be identified within distinct functional networks including SM and VIS networks. Similar patterns of functional connectivity were consistently evident across many functional network studies (Diez-Cirarda et al., 2018; Kim et al., 2017; Schumacher et al., 2019; Wang et al., 2015a). As stated above, in our study, the altered functional connectivity state of sensory-motor networks was closely linked to physical weakness. Previously, a study in cognitively normal older adults evaluated resting state connectivity in cortical motor regions and found stronger connectivity with greater grip strength (Seidler et al., 2015). The recruitment and activation of motor-related regions within the network are crucial for the performance during the motor task, and the functional connectivity even at rest is known to be highly predictive of brain activations during the task performance (Langan et al., 2010). Taken together,

the altered temporal features of State 1 observed in our study may underlie the physical impairments in MCI with frailty.

State 2 can be characterized by stronger connectivity within DM network and anti-correlated couplings between DM and sensory networks, and its expression was accompanied with poor cognitive function measured by MMSE-K. There is a general consensus that DM network is implicated in higher-order cognitive functions and self-referential processing and is highly activated during resting state in counter-phase with other functional networks (Greicius, Krasnow, Reiss, & Menon, 2003). The anti-correlated interactions between DM and sensorimotor networks are essential for effective cognitive processing, and intensive functional studies have proved disruptions of DM network in MCI and AD (Christopher et al., 2015; Greicius, Srivastava, Reiss, & Menon, 2004; Sorg et al., 2007; Wang et al., 2015a; Zhu, Majumdar, Korolev, Berger, & Bozoki, 2013). In the current results, the overexpression of interactions between DM and sensorimotor networks may interfere with network functional specializations, which lead to lower MMSE-K score in MCI.

Analyses of functional connectivity strength changes between network components displayed that functional connectivity between SM and CC was weakened in at-risk group. On the other hand, the connectivity between VIS and DM network was heightened. Generally, sensorimotor networks which receive external signals convey the signals to attention or cognitive control system to interpret the information and induce appropriate responses (Wang et al., 2015a). The alterations of functional connectivity between sensorimotor and cognitive networks may reflect disrupted communications that are normally required for effective cognitive processing of sensorimotor signals. Over decades, sensorimotor

network has been thought to remain relatively stable in MCI and AD (Li et al., 2002; Wang et al., 2012; Wang et al., 2015a), however, recent work demonstrated dysfunctional interactions of sensorimotor networks involving motor and visual systems (Albers et al., 2015; Cai et al., 2017; Wang et al., 2015a). Hyper-connectivity within CC network has also been observed in at-risk group, and it may represent a network reconfiguration to compensate, for the reduced functional segregation reported beforehand, to preserve daily abilities that are relatively intact in early stages of MCI. Accordingly, basal functional hyperactivity is often observed at the initiation of AD-related pathological processes in MCI, which protects against the disease and provides the capacity to withstand deposition of AD pathology and to maintain normal cognitive functioning (Cohen et al., 2009; Joo, Lim, & Lee, 2016).

The graph theory-based analyses showed that temporal variations in global and local efficiency of functional networks were not significantly different between at-risk and robust groups. A higher variability in network efficiency represents inefficient and unstable information transfer between and within brain networks. Although the breakdown of network functional segregation was apparent in association with physical weakness, the network efficiencies were not significantly compromised, possibly due to the compensatory network reconfigurations observed.

There has been an extensive debate regarding the functional significance and the reliability of dynamic functional connectivity analysis. It still remains to be discovered what dynamic intrinsic network represents in regards with cognitive functioning. The dynamic revolutions of brain networks may to some extent mirror instant cognitive activities, but also reflect intrinsic physiological properties to

some other extent. However, a simultaneous fMRI and electroencephalography study by Chang, Liu, Chen, Liu, and Duyn (2013) has demonstrated an electrical origin of time-varying functional connectivity, and several lines of evidence also determined temporal changes in functional connectivity in relation to behavior (Jia, Hu, & Deshpande, 2014; Kucyi, Hove, Esterman, Hutchison, & Valera, 2017; Thompson et al., 2013). Furthermore, it has been proved that dynamic states were affected by pathological conditions (Damaraju et al., 2014; Kim et al., 2017; Rashid, Damaraju, Pearlson, & Calhoun, 2014).

Overall, abnormal dynamic functional network patterns which reflect reduced functional segregation of brain networks in associations with physical and cognitive deficits were found. Also, functional reconfigurations of sensorimotor and cognitive networks were found in cognitive frailty.

5.3 Conclusion and limitations of the study

The current study demonstrated metabolic and functional abnormalities in brain regions, where are implicated in various cognitive processes including executive, visuospatial, and language functions, in associations with physical frailty in MCI. Abnormal temporal functional network patterns were also coupled with physical weakness and poorer cognitive function, which provide new insights into the role of dynamic functional connectivity as a potential neuroimaging biomarker in MCI with frailty.

In the present study, among physical frailty measures, grip strength was a strong indicator of neural activity changes and network reconfigurations observed in cognitive frailty patients. It has been shown that the muscle strength was substantially associated with the risk of cognitive deficits and development of AD,

and thus, it suggests that assessment of muscle strength may be of diagnostic utility to identify individuals at risk of cognitive decline (Boyle, Buchman, Wilson, Leurgans, & Bennett, 2009; Boyle et al., 2010). Although the underlying basis of the association between cognitive impairments and muscle strength is uncertain, it can be speculated that the underlying aging or disease processes which cause mitochondrial dysfunction result in the loss of muscle strength and muscle-generated energy production (Boyle et al., 2009). This may consequently affect the brain and cognitive functioning. There has been a great consensus that physical exercise improves cognition and wellbeing by reinforcing brain plasticity (Colcombe & Kramer, 2003; Fernandes, Arida, & Gomez-Pinilla, 2017; Mandolesi et al., 2018). In fact, there is evidence that exercise induces biochemical and structural changes in the brain, and such changes are reflected on cognitive functioning (Fernandes et al., 2017; Mandolesi et al., 2018). In this regard, aerobic exercise was associated with enhanced functional and structural integrity in brain regions that are affected in aging process, such as frontal and temporal cortices, and in regions that are collaborated in motor function (Adlard, Perreau, & Cotman, 2005; Colcombe & Kramer, 2003; Colcombe et al., 2006; Colcombe et al., 2004; Erickson et al., 2009; Pereira et al., 2007; Voss et al., 2010), and it was associated with improvements in cognitive abilities coordinated by those affected regions (Colcombe & Kramer, 2003; Colcombe et al., 2004; Pereira et al., 2007). Although the neurobiological mechanisms of cognitive improvements following physical exercise, literature demonstrated that physical exercise facilitates the release of neurotrophic factors and increases blood flow and glucose metabolism, which benefits the brain functioning (Hotting, Schickert, Kaiser, Roder, & Schmidt-Kassow, 2016; Mandolesi et al., 2017). It is likely that physical exercise promotes

blood circulation and synaptic plasticity in the neural circuits implicated in cognitive processes (Erickson, Gildengers, & Butters, 2013; Mandolesi et al., 2018; Voss et al., 2010). Also, improved physical function may permit to gain cognitive and brain reserves in cases of normal ageing and neurodegenerative diseases (Chang et al., 2010; Loprinzi, Frith, Edwards, Sng, & Ashpole, 2018; Mandolesi et al., 2018).

There are a few limitations that need to be considered for the current study results. First of all, at-risk group included mostly pre-frail individuals who may be at a transitional/intermediate phase to frailty, which may have hampered clear observations of characteristics of neural activity changes. This may have led to a low statistical power in the neuroimaging results. Secondly, all the findings are based on cross-sectional data, and cannot be interpreted as causal. Stemming from this point, our at-risk cohort may include those whose physical impairment occurred following cognitive decline. For example, physical dysfunction is often reported in patients with cognitive impairments due to obstacles in daily activities and impaired motor learning originating from cognitive dysfunction (Ruan et al., 2015). In such cases, the pathological mechanisms may be different from the others with the other way around. Furthermore, the influences of AD-related genetic factors (such as APOE-4 gene) and cardiovascular risk factors on functional alterations in cognitive frailty need to be taken into consideration in larger samples. Moreover, the criteria of frailty included categorical variables (the presence of weight loss, the presence of exhaustion) which limited the explorations of associations of those variables with the metabolic and functional activities and with the dynamic properties of functional network connectivity. Additional continuous measurements to examine the weight loss and exhaustion may provide a more

complete view of the pathophysiological mechanisms of cognitive frailty. Finally, the parameters of rs-fMRI acquisition can be problematic when it comes to dynamic functional connectivity analysis. The temporal resolution (i.e. repetition time) and length of data acquisition should be improved for a better reliability of the results that mirror the dynamics of fluctuations. Also, a priori specification of analysis parameters such as the length of window and the number of states can be another problematic aspect of the dynamic approach employed in the current study.

References

Adlard, P. A., Perreau, V. M., & Cotman, C. W. (2005). The exercise-induced expression of BDNF within the hippocampus varies across life-span. *Neurobiol Aging, 26*(4), 511-520.

Albers, M. W., Gilmore, G. C., Kaye, J., Murphy, C., Wingfield, A., Bennett, D. A., . . . Zhang, L. I. (2015). At the interface of sensory and motor dysfunctions and Alzheimer's disease. *Alzheimers Dement, 11*(1), 70-98.

Albert, M. S., DeKosky, S. T., Dickson, D., Dubois, B., Feldman, H. H., Fox, N. C., . . . Phelps, C. H. (2011). The diagnosis of mild cognitive impairment due to Alzheimer's disease: recommendations from the National Institute on Aging-Alzheimer's Association workgroups on diagnostic guidelines for Alzheimer's disease. *Alzheimers Dement, 7*(3), 270-279.

Allen, E. A., Damaraju, E., Plis, S. M., Erhardt, E. B., Eichele, T., & Calhoun, V. D. (2014). Tracking whole-brain connectivity dynamics in the resting state. *Cereb Cortex, 24*(3), 663-676.

Andrews-Hanna, J. R., Snyder, A. Z., Vincent, J. L., Lustig, C., Head, D., Raichle, M. E., & Buckner, R. L. (2007). Disruption of large-scale brain systems in advanced aging. *Neuron, 56*(5), 924-935.

Ardila, A., Bernal, B., & Rosselli, M. (2014). The Elusive Role of the Left Temporal Pole (BA38) in Language: A Preliminary Meta-Analytic Connectivity Study. *International Journal of Brain Science, 2014*, 7.

Armstrong, J. J., Stolee, P., Hirdes, J. P., & Poss, J. W. (2010). Examining three frailty conceptualizations in their ability to predict negative outcomes for home-care clients. *Age and Ageing, 39*(6), 755-758.

Arnaiz, E., Jelic, V., Almkvist, O., Wahlund, L. O., Winblad, B., Valind, S., & Nordberg, A. (2001). Impaired cerebral glucose metabolism and cognitive functioning predict deterioration in mild cognitive impairment. *Neuroreport, 12*(4), 851-855.

Arnold, S. E., Hyman, B. T., Flory, J., Damasio, A. R., & Van Hoesen, G. W. (1991). The topographical and neuroanatomical distribution of neurofibrillary tangles and neuritic plaques in the cerebral cortex of patients with Alzheimer's disease. *Cereb Cortex, 1*(1), 103-116.

Avila-Funes, J. A., Pelletier, A., Meillon, C., Catheline, G., Periot, O., Trevin, O. F. I., . . . Amieva, H. (2017). Vascular Cerebral Damage in Frail Older Adults: The AMImage Study. *J Gerontol A Biol Sci Med Sci, 72*(7), 971-977.

Biswal, B., Yetkin, F. Z., Haughton, V. M., & Hyde, J. S. (1995). Functional connectivity in the motor cortex of resting human brain using echo-planar MRI. *Magn Reson Med, 34*(4), 537-541.

Biswal, B. B., Van Kylen, J., & Hyde, J. S. (1997). Simultaneous assessment of flow and BOLD signals in resting-state functional connectivity maps. *NMR Biomed, 10*(4-5), 165-170.

Boyle, P. A., Buchman, A. S., Wilson, R. S., Leurgans, S. E., & Bennett, D. A. (2009). Association of muscle strength with the risk of Alzheimer disease and the rate of cognitive decline in community-dwelling older persons. *Arch Neurol, 66*(11), 1339-1344.

Boyle, P. A., Buchman, A. S., Wilson, R. S., Leurgans, S. E., & Bennett, D. A. (2010). Physical frailty is associated with incident mild cognitive impairment in community-based older persons. *J Am Geriatr Soc, 58*(2), 248-255.

Buchman, A. S., Boyle, P. A., Wilson, R. S., Tang, Y., & Bennett, D. A. (2007). Frailty is associated with incident Alzheimer's disease and cognitive decline in the elderly. *Psychosom Med, 69*(5), 483-489.

Buchman, A. S., Schneider, J. A., Leurgans, S., & Bennett, D. A. (2008). Physical frailty in older persons is associated with Alzheimer disease pathology. *Neurology, 71*(7), 499-504.

Buchman, A. S., Yu, L., Wilson, R. S., Boyle, P. A., Schneider, J. A., & Bennett, D. A. (2014). Brain pathology contributes to simultaneous change in physical frailty and cognition in old age. *J Gerontol A Biol Sci Med Sci, 69*(12), 1536-1544.

Byun, M. S., Yi, D., Lee, J. H., Choe, Y. M., Sohn, B. K., Lee, J. Y., . . . Group, K. R. (2017). Korean Brain Aging Study for the Early Diagnosis and Prediction of Alzheimer's Disease: Methodology and Baseline Sample Characteristics. *Psychiatry Investig, 14*(6), 851-863.

Cai, S., Chong, T., Peng, Y., Shen, W., Li, J., von Deneen, K. M., . . . Alzheimer's Disease Neuroimaging, I. (2017). Altered functional brain networks in

amnestic mild cognitive impairment: a resting-state fMRI study. *Brain Imaging Behav, 11*(3), 619-631.

Calhoun, V. D., Adali, T., Pearlson, G. D., & Pekar, J. J. (2001). A method for making group inferences from functional MRI data using independent component analysis. *Hum Brain Mapp, 14*(3), 140-151.

Calhoun, V. D., Liu, J., & Adali, T. (2009). A review of group ICA for fMRI data and ICA for joint inference of imaging, genetic, and ERP data. *Neuroimage, 45*(1 Suppl), S163-172.

Calhoun, V. D., Miller, R., Pearlson, G., & Adali, T. (2014). The chronnectome: time-varying connectivity networks as the next frontier in fMRI data discovery. *Neuron, 84*(2), 262-274.

Camicioli, R., Moore, M. M., Sexton, G., Howieson, D. B., & Kaye, J. A. (1999). Age-related brain changes associated with motor function in healthy older people. *J Am Geriatr Soc, 47*(3), 330-334.

Carmelli, D., DeCarli, C., Swan, G. E., Kelly-Hayes, M., Wolf, P. A., Reed, T., & Guralnik, J. M. (2000). The joint effect of apolipoprotein E epsilon4 and MRI findings on lower-extremity function and decline in cognitive function. *J Gerontol A Biol Sci Med Sci, 55*(2), M103-109.

Cavanna, A. E., & Trimble, M. R. (2006). The precuneus: a review of its functional anatomy and behavioural correlates. *Brain, 129*(Pt 3), 564-583.

Chan, M. Y., Park, D. C., Savalia, N. K., Petersen, S. E., & Wig, G. S. (2014). Decreased segregation of brain systems across the healthy adult lifespan. *Proc Natl Acad Sci U S A, 111*(46), E4997-5006.

Chang, C., & Glover, G. H. (2010). Time-frequency dynamics of resting-state brain connectivity measured with fMRI. *Neuroimage, 50*(1), 81-98.

Chang, C., Liu, Z., Chen, M. C., Liu, X., & Duyn, J. H. (2013). EEG correlates of time-varying BOLD functional connectivity. *Neuroimage, 72*, 227-236.

Chang, M., Jonsson, P. V., Snaedal, J., Bjornsson, S., Saczynski, J. S., Aspelund, T., . . . Launer, L. J. (2010). The effect of midlife physical activity on cognitive function among older adults: AGES--Reykjavik Study. *J Gerontol A Biol Sci Med Sci, 65*(12), 1369-1374.

Chen, W. T., Chou, K. H., Liu, L. K., Lee, P. L., Lee, W. J., Chen, L. K., . . . Lin, C. P. (2015). Reduced cerebellar gray matter is a neural signature of physical frailty. *Hum Brain Mapp, 36*(9), 3666-3676.

Chen, X., Zhang, H., Zhang, L., Shen, C., Lee, S. W., & Shen, D. (2017). Extraction of dynamic functional connectivity from brain grey matter and white matter for MCI classification. *Hum Brain Mapp, 38*(10), 5019-5034.

Chetelat, G., Desgranges, B., de la Sayette, V., Viader, F., Eustache, F., & Baron, J. C. (2003). Mild cognitive impairment: Can FDG-PET predict who is to rapidly convert to Alzheimer's disease? *Neurology, 60*(8), 1374-1377.

Chetelat, G., Eustache, F., Viader, F., De La Sayette, V., Pelerin, A., Mezenge, F., . . . Desgranges, B. (2005). FDG-PET measurement is more accurate than neuropsychological assessments to predict global cognitive deterioration in patients with mild cognitive impairment. *Neurocase, 11*(1), 14-25.

Christopher, L., Duff-Canning, S., Koshimori, Y., Segura, B., Boileau, I., Chen, R., . . . Strafella, A. P. (2015). Salience network and parahippocampal dopamine dysfunction in memory-impaired Parkinson disease. *Ann Neurol, 77*(2), 269-280.

Cohen, A. D., Price, J. C., Weissfeld, L. A., James, J., Rosario, B. L., Bi, W., . . . Klunk, W. E. (2009). Basal cerebral metabolism may modulate the cognitive effects of Abeta in mild cognitive impairment: an example of brain reserve. *J Neurosci, 29*(47), 14770-14778.

Colcombe, S., & Kramer, A. F. (2003). Fitness effects on the cognitive function of older adults: a meta-analytic study. *Psychol Sci, 14*(2), 125-130.

Colcombe, S. J., Erickson, K. I., Scalf, P. E., Kim, J. S., Prakash, R., McAuley, E., . . . Kramer, A. F. (2006). Aerobic exercise training increases brain volume in aging humans. *J Gerontol A Biol Sci Med Sci, 61*(11), 1166-1170.

Colcombe, S. J., Kramer, A. F., Erickson, K. I., Scalf, P., McAuley, E., Cohen, N. J., . . . Elavsky, S. (2004). Cardiovascular fitness, cortical plasticity, and aging. *Proc Natl Acad Sci U S A, 101*(9), 3316-3321.

Corbetta, M., & Shulman, G. L. (2002). Control of goal-directed and stimulus-driven attention in the brain. *Nat Rev Neurosci, 3*(3), 201-215.

Craig, C. L., Marshall, A. L., Sjostrom, M., Bauman, A. E., Booth, M. L., Ainsworth, B. E., . . . Oja, P. (2003). International physical activity questionnaire: 12-country reliability and validity. *Med Sci Sports Exerc, 35*(8), 1381-1395.

Crinion, J., Turner, R., Grogan, A., Hanakawa, T., Noppeney, U., Devlin, J. T., . . . Price, C. J. (2006). Language control in the bilingual brain. *Science, 312*(5779), 1537-1540.

Damaraju, E., Allen, E. A., Belger, A., Ford, J. M., McEwen, S., Mathalon, D. H., . . . Calhoun, V. D. (2014). Dynamic functional connectivity analysis reveals transient states of dysconnectivity in schizophrenia. *Neuroimage Clin, 5*, 298-308.

Diez-Cirarda, M., Strafella, A. P., Kim, J., Pena, J., Ojeda, N., Cabrera-Zubizarreta, A., & Ibarretxe-Bilbao, N. (2018). Dynamic functional connectivity in Parkinson's disease patients with mild cognitive impairment and normal cognition. *Neuroimage Clin, 17*, 847-855.

Ding, S. L., Van Hoesen, G. W., Cassell, M. D., & Poremba, A. (2009). Parcellation of human temporal polar cortex: a combined analysis of multiple cytoarchitectonic, chemoarchitectonic, and pathological markers. *J Comp Neurol, 514*(6), 595-623.

Elman, J. A., Madison, C. M., Baker, S. L., Vogel, J. W., Marks, S. M., Crowley, S., . . . Jagust, W. J. (2016). Effects of Beta-Amyloid on Resting State Functional Connectivity Within and Between Networks Reflect Known Patterns of Regional Vulnerability. *Cereb Cortex, 26*(2), 695-707.

Erickson, K. I., Gildengers, A. G., & Butters, M. A. (2013). Physical activity and brain plasticity in late adulthood. *Dialogues Clin Neurosci, 15*(1), 99-108.

Erickson, K. I., Prakash, R. S., Voss, M. W., Chaddock, L., Hu, L., Morris, K. S., . . . Kramer, A. F. (2009). Aerobic fitness is associated with hippocampal volume in elderly humans. *Hippocampus, 19*(10), 1030-1039.

Fernandes, J., Arida, R. M., & Gomez-Pinilla, F. (2017). Physical exercise as an epigenetic modulator of brain plasticity and cognition. *Neurosci Biobehav Rev, 80*, 443-456.

Fried, L. P., Borhani, N. O., Enright, P., Furberg, C. D., Gardin, J. M., Kronmal, R. A., . . . et al. (1991). The Cardiovascular Health Study: design and rationale. *Ann Epidemiol, 1*(3), 263-276.

Fried, L. P., Tangen, C. M., Walston, J., Newman, A. B., Hirsch, C., Gottdiener, J., . . . Cardiovascular Health Study Collaborative Research, G. (2001). Frailty in older adults: evidence for a phenotype. *J Gerontol A Biol Sci Med Sci, 56*(3), M146-156.

Ghanavati, E., Salehinejad, M. A., Nejati, V., & Nitsche, M. A. (2019). Differential role of prefrontal, temporal and parietal cortices in verbal and figural fluency: Implications for the supramodal contribution of executive functions. *Sci Rep, 9*(1), 3700.

Gil Robles, S., Gatignol, P., Capelle, L., Mitchell, M. C., & Duffau, H. (2005). The role of dominant striatum in language: a study using intraoperative electrical stimulations. *J Neurol Neurosurg Psychiatry, 76*(7), 940-946.

Gray, S. L., Anderson, M. L., Hubbard, R. A., LaCroix, A., Crane, P. K., McCormick, W., . . . Larson, E. B. (2013). Frailty and incident dementia. *J Gerontol A Biol Sci Med Sci, 68*(9), 1083-1090.

Greicius, M. D., Krasnow, B., Reiss, A. L., & Menon, V. (2003). Functional connectivity in the resting brain: a network analysis of the default mode hypothesis. *Proc Natl Acad Sci U S A, 100*(1), 253-258.

Greicius, M. D., Srivastava, G., Reiss, A. L., & Menon, V. (2004). Default-mode network activity distinguishes Alzheimer's disease from healthy aging: evidence from functional MRI. *Proc Natl Acad Sci U S A, 101*(13), 4637-4642.

Gronholm, E. O., Roll, M. C., Horne, M. A., Sundgren, P. C., & Lindgren, A. G. (2016). Predominance of caudate nucleus lesions in acute ischaemic stroke patients with impairment in language and speech. *Eur J Neurol, 23*(1), 148-153.

Gurd, J. M., Amunts, K., Weiss, P. H., Zafiris, O., Zilles, K., Marshall, J. C., & Fink, G. R. (2002). Posterior parietal cortex is implicated in continuous switching between verbal fluency tasks: an fMRI study with clinical implications. *Brain, 125*(Pt 5), 1024-1038.

Haxby, J. V., Grady, C. L., Koss, E., Horwitz, B., Heston, L., Schapiro, M., . . . Rapoport, S. I. (1990). Longitudinal study of cerebral metabolic asymmetries and associated neuropsychological patterns in early dementia of the Alzheimer type. *Arch Neurol, 47*(7), 753-760.

Hillis, A. E., Barker, P. B., Wityk, R. J., Aldrich, E. M., Restrepo, L., Breese, E. L., & Work, M. (2004). Variability in subcortical aphasia is due to variable sites of cortical hypoperfusion. *Brain Lang, 89*(3), 524-530.

Hotting, K., Schickert, N., Kaiser, J., Roder, B., & Schmidt-Kassow, M. (2016). The Effects of Acute Physical Exercise on Memory, Peripheral BDNF, and Cortisol in Young Adults. *Neural Plast, 2016*, 6860573.

Hutchison, R. M., Womelsdorf, T., Allen, E. A., Bandettini, P. A., Calhoun, V. D., Corbetta, M., . . . Chang, C. (2013). Dynamic functional connectivity: promise, issues, and interpretations. *Neuroimage, 80*, 360-378.

Ishii, K. (2014). PET approaches for diagnosis of dementia. *AJNR Am J Neuroradiol, 35*(11), 2030-2038.

Jia, H., Hu, X., & Deshpande, G. (2014). Behavioral relevance of the dynamics of the functional brain connectome. *Brain Connect, 4*(9), 741-759.

Joo, S. H., Lim, H. K., & Lee, C. U. (2016). Three Large-Scale Functional Brain Networks from Resting-State Functional MRI in Subjects with Different Levels of Cognitive Impairment. *Psychiatry Investig, 13*(1), 1-7.

Jung, H. W., Kim, S. W., Ahn, S., Lim, J. Y., Han, J. W., Kim, T. H., . . . Kim, C. H. (2014a). Prevalence and outcomes of frailty in Korean elderly population: comparisons of a multidimensional frailty index with two phenotype models. *PLoS One, 9*(2), e87958.

Jung, H. W., Kim, S. W., Yoon, S. J., Choi, J. Y., Kim, K. I., & Kim, C. H. (2014b). Associations between frailty, retinal microvascular changes, and cerebral white matter abnormalities in Korean older adults. *J Am Geriatr Soc, 62*(11), 2209-2210.

Kaiser, R. H., Whitfield-Gabrieli, S., Dillon, D. G., Goer, F., Beltzer, M., Minkel, J., . . . Pizzagalli, D. A. (2016). Dynamic Resting-State Functional Connectivity in Major Depression. *Neuropsychopharmacology, 41*(7), 1822-1830.

Kelaiditi, E., Cesari, M., Canevelli, M., van Kan, G. A., Ousset, P. J., Gillette-Guyonnet, S., . . . Iana/Iagg. (2013). Cognitive frailty: rational and definition from an (I.A.N.A./I.A.G.G.) international consensus group. *J Nutr Health Aging, 17*(9), 726-734.

Kilintari, M., Raos, V., & Savaki, H. E. (2014). Involvement of the superior temporal cortex in action execution and action observation. *J Neurosci, 34*(27), 8999-9011.

Kim, J., Criaud, M., Cho, S. S., Diez-Cirarda, M., Mihaescu, A., Coakeley, S., . . . Strafella, A. P. (2017). Abnormal intrinsic brain functional network dynamics in Parkinson's disease. *Brain, 140*(11), 2955-2967.

Kimberg, D. Y., Aguirre, G. K., & D'Esposito, M. (2000). Modulation of task-related neural activity in task-switching: an fMRI study. *Brain Res Cogn Brain Res, 10*(1-2), 189-196.

Kiviniemi, V., Starck, T., Remes, J., Long, X., Nikkinen, J., Haapea, M., . . . Tervonen, O. (2009). Functional segmentation of the brain cortex using high model order group PICA. *Hum Brain Mapp, 30*(12), 3865-3886.

Koenigs, M., Barbey, A. K., Postle, B. R., & Grafman, J. (2009). Superior parietal cortex is critical for the manipulation of information in working memory. *J Neurosci, 29*(47), 14980-14986.

Kucyi, A., Hove, M. J., Esterman, M., Hutchison, R. M., & Valera, E. M. (2017). Dynamic Brain Network Correlates of Spontaneous Fluctuations in Attention. *Cereb Cortex, 27*(3), 1831-1840.

Langan, J., Peltier, S. J., Bo, J., Fling, B. W., Welsh, R. C., & Seidler, R. D. (2010). Functional implications of age differences in motor system connectivity. *Front Syst Neurosci, 4*, 17.

Langlois, F., Vu, T. T., Kergoat, M. J., Chasse, K., Dupuis, G., & Bherer, L. (2012). The multiple dimensions of frailty: physical capacity, cognition, and quality of life. *Int Psychogeriatr, 24*(9), 1429-1436.

Li, S. J., Li, Z., Wu, G., Zhang, M. J., Franczak, M., & Antuono, P. G. (2002). Alzheimer Disease: evaluation of a functional MR imaging index as a marker. *Radiology, 225*(1), 253-259.

Lloyd, S. P. (1982). Least-Squares Quantization in Pcm. *Ieee Transactions on Information Theory, 28*(2), 129-137.

Loprinzi, P. D., Frith, E., Edwards, M. K., Sng, E., & Ashpole, N. (2018). The Effects of Exercise on Memory Function Among Young to Middle-Aged Adults: Systematic Review and Recommendations for Future Research. *Am J Health Promot, 32*(3), 691-704.

Maltais, M., de Souto Barreto, P., Hooper, C., Payoux, P., Rolland, Y., Vellas, B., & Group, M. D. S. (2019). Association between brain -amyloid and frailty in older adults. *J Gerontol A Biol Sci Med Sci*.

Mandolesi, L., Gelfo, F., Serra, L., Montuori, S., Polverino, A., Curcio, G., & Sorrentino, G. (2017). Environmental Factors Promoting Neural Plasticity: Insights from Animal and Human Studies. *Neural Plast, 2017*, 7219461.

Mandolesi, L., Polverino, A., Montuori, S., Foti, F., Ferraioli, G., Sorrentino, P., & Sorrentino, G. (2018). Effects of Physical Exercise on Cognitive Functioning and Wellbeing: Biological and Psychological Benefits. *Front Psychol, 9*, 509.

Marchitelli, R., Aiello, M., Cachia, A., Quarantelli, M., Cavaliere, C., Postiglione, A., . . . Pappata, S. (2018). Simultaneous resting-state FDG-PET/fMRI in Alzheimer Disease: Relationship between glucose metabolism and intrinsic activity. *Neuroimage, 176*, 246-258.

Matsuda, H. (2001). Cerebral blood flow and metabolic abnormalities in Alzheimer's disease. *Ann Nucl Med, 15*(2), 85-92.

Mosconi, L. (2005). Brain glucose metabolism in the early and specific diagnosis of Alzheimer's disease. FDG-PET studies in MCI and AD. *Eur J Nucl Med Mol Imaging, 32*(4), 486-510.

Newman, A. B., Gottdiener, J. S., McBurnie, M. A., Hirsch, C. H., Kop, W. J., Tracy, R., . . . Cardiovascular Health Study Research, G. (2001). Associations of subclinical cardiovascular disease with frailty. *J Gerontol A Biol Sci Med Sci, 56*(3), M158-166.

Orme, J. G., Reis, J., & Herz, E. J. (1986). Factorial and discriminant validity of the Center for Epidemiological Studies Depression (CES-D) scale. *J Clin Psychol, 42*(1), 28-33.

Panza, F., D'Introno, A., Colacicco, A. M., Capurso, C., Parigi, A. D., Capurso, S. A., . . . Solfrizzi, V. (2006). Cognitive frailty: Predementia syndrome and vascular risk factors. *Neurobiol Aging, 27*(7), 933-940.

Panza, F., Lozupone, M., Solfrizzi, V., Sardone, R., Dibello, V., Di Lena, L., . . . Logroscino, G. (2018). Different Cognitive Frailty Models and Health- and Cognitive-related Outcomes in Older Age: From Epidemiology to Prevention. *J Alzheimers Dis, 62*(3), 993-1012.

Panza, F., Solfrizzi, V., Frisardi, V., Maggi, S., Sancarlo, D., Adante, F., . . . Pilotto, A. (2011). Different models of frailty in predementia and dementia syndromes. *J Nutr Health Aging, 15*(8), 711-719.

Patrick, L., Gaskovski, P., & Rexroth, D. (2002). Cumulative illness and neuropsychological decline in hospitalized geriatric patients. *Clin Neuropsychol, 16*(2), 145-156.

Pereira, A. C., Huddleston, D. E., Brickman, A. M., Sosunov, A. A., Hen, R., McKhann, G. M., . . . Small, S. A. (2007). An in vivo correlate of exercise-induced neurogenesis in the adult dentate gyrus. *Proc Natl Acad Sci U S A, 104*(13), 5638-5643.

Preti, M. G., Bolton, T. A., & Van De Ville, D. (2017). The dynamic functional connectome: State-of-the-art and perspectives. *Neuroimage, 160*, 41-54.

Raichle, M. E., MacLeod, A. M., Snyder, A. Z., Powers, W. J., Gusnard, D. A., & Shulman, G. L. (2001). A default mode of brain function. *Proc Natl Acad Sci U S A, 98*(2), 676-682.

Rashid, B., Damaraju, E., Pearlson, G. D., & Calhoun, V. D. (2014). Dynamic connectivity states estimated from resting fMRI Identify differences among Schizophrenia, bipolar disorder, and healthy control subjects. *Front Hum Neurosci, 8*, 897.

Robertson, D. A., Savva, G. M., & Kenny, R. A. (2013). Frailty and cognitive impairment--a review of the evidence and causal mechanisms. *Ageing Res Rev, 12*(4), 840-851.

Rosano, C., Aizenstein, H. J., Studenski, S., & Newman, A. B. (2007). A regions-of-interest volumetric analysis of mobility limitations in community-dwelling older adults. *J Gerontol A Biol Sci Med Sci, 62*(9), 1048-1055.

Rosano, C., Kuller, L. H., Chung, H., Arnold, A. M., Longstreth, W. T., Jr., & Newman, A. B. (2005). Subclinical brain magnetic resonance imaging abnormalities predict physical functional decline in high-functioning older adults. *J Am Geriatr Soc, 53*(4), 649-654.

Rosano, C., Sigurdsson, S., Siggeirsdottir, K., Phillips, C. L., Garcia, M., Jonsson, P. V., . . . Launer, L. J. (2010). Magnetization transfer imaging, white matter hyperintensities, brain atrophy and slower gait in older men and women. *Neurobiol Aging, 31*(7), 1197-1204.

Ruan, Q., Yu, Z., Chen, M., Bao, Z., Li, J., & He, W. (2015). Cognitive frailty, a novel target for the prevention of elderly dependency. *Ageing Res Rev, 20*, 1-10.

Sakurai, R., Fujiwara, Y., Yasunaga, M., Takeuchi, R., Murayama, Y., Ohba, H., . . . Ishii, K. (2014). Regional cerebral glucose metabolism and gait speed in healthy community-dwelling older women. *J Gerontol A Biol Sci Med Sci, 69*(12), 1519-1527.

Schneider, J. A., Li, J. L., Li, Y., Wilson, R. S., Kordower, J. H., & Bennett, D. A. (2006). Substantia nigra tangles are related to gait impairment in older persons. *Ann Neurol, 59*(1), 166-173.

Schumacher, J., Peraza, L. R., Firbank, M., Thomas, A. J., Kaiser, M., Gallagher, P., . . . Taylor, J. P. (2019). Dynamic functional connectivity changes in dementia with Lewy bodies and Alzheimer's disease. *Neuroimage Clin, 22*, 101812.

Seeley, W. W., Crawford, R. K., Zhou, J., Miller, B. L., & Greicius, M. D. (2009). Neurodegenerative diseases target large-scale human brain networks. *Neuron, 62*(1), 42-52.

Seeley, W. W., Menon, V., Schatzberg, A. F., Keller, J., Glover, G. H., Kenna, H., . . . Greicius, M. D. (2007). Dissociable intrinsic connectivity networks for salience processing and executive control. *J Neurosci, 27*(9), 2349-2356.

Seidler, R., Erdeniz, B., Koppelmans, V., Hirsiger, S., Merillat, S., & Jancke, L. (2015). Associations between age, motor function, and resting state sensorimotor network connectivity in healthy older adults. *Neuroimage, 108*, 47-59.

Shen, Z., Jiang, L., Yang, S., Ye, J., Dai, N., Liu, X., . . . Xu, X. (2017). Identify changes of brain regional homogeneity in early and later adult onset patients with first-episode depression using resting-state fMRI. *PLoS One, 12*(9), e0184712.

Shim, E. Y., Ma, S. H., Hong, S. H., Lee, Y. S., Paik, W. Y., Seo, D. S., . . . Yoon, J. L. (2011). Correlation between Frailty Level and Adverse Health-related Outcomes of Community-Dwelling Elderly, One Year Retrospective Study. *Korean journal of family medicine, 32*(4), 249-256.

Shimada, H., Ishii, K., Ishiwata, K., Oda, K., Suzukawa, M., Makizako, H., . . . Suzuki, T. (2013). Gait adaptability and brain activity during unaccustomed treadmill walking in healthy elderly females. *Gait Posture, 38*(2), 203-208.

Small, G. W., Ercoli, L. M., Silverman, D. H., Huang, S. C., Komo, S., Bookheimer, S. Y., . . . Phelps, M. E. (2000). Cerebral metabolic and cognitive decline in persons at genetic risk for Alzheimer's disease. *Proc Natl Acad Sci U S A, 97*(11), 6037-6042.

Sohn, M. H., Ursu, S., Anderson, J. R., Stenger, V. A., & Carter, C. S. (2000). The role of prefrontal cortex and posterior parietal cortex in task switching. *Proc Natl Acad Sci U S A, 97*(24), 13448-13453.

Sorg, C., Riedl, V., Muhlau, M., Calhoun, V. D., Eichele, T., Laer, L., . . . Wohlschlager, A. M. (2007). Selective changes of resting-state networks in individuals at risk for Alzheimer's disease. *Proc Natl Acad Sci U S A, 104*(47), 18760-18765.

Sourty, M., Thoraval, L., Roquet, D., Armspach, J. P., Foucher, J., & Blanc, F. (2016). Identifying Dynamic Functional Connectivity Changes in Dementia with Lewy Bodies Based on Product Hidden Markov Models. *Front Comput Neurosci, 10*, 60.

Sporns, O. (2013). Network attributes for segregation and integration in the human brain. *Curr Opin Neurobiol, 23*(2), 162-171.

Thompson, G. J., Magnuson, M. E., Merritt, M. D., Schwarb, H., Pan, W. J., McKinley, A., . . . Keilholz, S. D. (2013). Short-time windows of correlation between large-scale functional brain networks predict vigilance intraindividually and interindividually. *Hum Brain Mapp, 34*(12), 3280-3298.

van den Heuvel, M. P., & Hulshoff Pol, H. E. (2010). Exploring the brain network: a review on resting-state fMRI functional connectivity. *Eur Neuropsychopharmacol, 20*(8), 519-534.

Viviano, R. P., Raz, N., Yuan, P., & Damoiseaux, J. S. (2017). Associations between dynamic functional connectivity and age, metabolic risk, and cognitive performance. *Neurobiol Aging, 59*, 135-143.

Voss, M. W., Prakash, R. S., Erickson, K. I., Basak, C., Chaddock, L., Kim, J. S., . . . Kramer, A. F. (2010). Plasticity of brain networks in a randomized intervention trial of exercise training in older adults. *Front Aging Neurosci, 2*.

Wang, B., Niu, Y., Miao, L., Cao, R., Yan, P., Guo, H., . . . Zhang, H. (2017). Decreased Complexity in Alzheimer's Disease: Resting-State fMRI Evidence of Brain Entropy Mapping. *Front Aging Neurosci, 9*, 378.

Wang, L., Roe, C. M., Snyder, A. Z., Brier, M. R., Thomas, J. B., Xiong, C., . . . Ances, B. M. (2012). Alzheimer disease family history impacts resting state functional connectivity. *Ann Neurol, 72*(4), 571-577.

Wang, P., Li, R., Yu, J., Huang, Z., & Li, J. (2016). Frequency-Dependent Brain Regional Homogeneity Alterations in Patients with Mild Cognitive Impairment during Working Memory State Relative to Resting State. *Front Aging Neurosci, 8*, 60.

Wang, P., Zhou, B., Yao, H., Zhan, Y., Zhang, Z., Cui, Y., . . . Jiang, T. (2015a). Aberrant intra- and inter-network connectivity architectures in Alzheimer's disease and mild cognitive impairment. *Sci Rep, 5*, 14824.

Wang, Y., Zhao, X., Xu, S., Yu, L., Wang, L., Song, M., . . . Wang, X. (2015b). Using regional homogeneity to reveal altered spontaneous activity in patients with mild cognitive impairment. *Biomed Res Int, 2015*, 807093.

Wennberg, A. M. V., Savica, R., Hagen, C. E., Roberts, R. O., Knopman, D. S., Hollman, J. H., . . . Mielke, M. M. (2017). Cerebral Amyloid Deposition Is Associated with Gait Parameters in the Mayo Clinic Study of Aging. *J Am Geriatr Soc, 65*(4), 792-799.

Wilkins, C. H., Roe, C. M., Morris, J. C., & Galvin, J. E. (2013). Mild physical impairment predicts future diagnosis of dementia of the Alzheimer's type. *J Am Geriatr Soc, 61*(7), 1055-1059.

Wu, T., Long, X., Zang, Y., Wang, L., Hallett, M., Li, K., & Chan, P. (2009). Regional homogeneity changes in patients with Parkinson's disease. *Hum Brain Mapp, 30*(5), 1502-1510.

Yoon, D. H., Lee, J. Y., Shin, S. A., Kim, Y. K., & Song, W. (2018). Physical Frailty and Amyloid-beta Deposits in the Brains of Older Adults with Cognitive Frailty. *J Clin Med, 7*(7).

Yu, Q., Erhardt, E. B., Sui, J., Du, Y., He, H., Hjelm, D., . . . Calhoun, V. D. (2015). Assessing dynamic brain graphs of time-varying connectivity in fMRI data: application to healthy controls and patients with schizophrenia. *Neuroimage, 107*, 345-355.

Yuan, J., Blumen, H. M., Verghese, J., & Holtzer, R. (2015). Functional connectivity associated with gait velocity during walking and walking-while-talking in aging: a resting-state fMRI study. *Hum Brain Mapp, 36*(4), 1484-1493.

Yuan, X., Han, Y., Wei, Y., Xia, M., Sheng, C., Jia, J., & He, Y. (2016). Regional homogeneity changes in amnestic mild cognitive impairment patients. *Neurosci Lett, 629*, 1-8.

Zang, Y., Jiang, T., Lu, Y., He, Y., & Tian, L. (2004). Regional homogeneity approach to fMRI data analysis. *Neuroimage, 22*(1), 394-400.

Zhang, Z., Liu, Y., Jiang, T., Zhou, B., An, N., Dai, H., . . . Zhang, X. (2012). Altered spontaneous activity in Alzheimer's disease and mild cognitive impairment revealed by Regional Homogeneity. *Neuroimage, 59*(2), 1429-1440.

Zhu, D. C., Majumdar, S., Korolev, I. O., Berger, K. L., & Bozoki, A. C. (2013). Alzheimer's disease and amnestic mild cognitive impairment weaken connections within the default-mode network: a multi-modal imaging study. *J Alzheimers Dis, 34*(4), 969-984.

국문 초록

인지 노쇠에서 FDG PET 과 휴지상태 fMRI 를 이용한 뇌 신경 활동과 기능적 연결성 패턴의 동적 변화 연구

신성아

의과학과 전공

서울대학교 대학원

인지 노쇠는 신체적 노쇠와 경도 인지 장애가 동시에 존재하는 것이 특징적인 최근 정의된 임상적 질환이다. 기존 연구에 의하면 신체적 노쇠와 인지 기능 저하는 공통적인 신경 병리적 기전을 가지는 것으로 알려져 있다. 또한, 신체적 기능 장애는 인지 기능 감소를 촉진하고, 나아가 알츠하이머병 치매 발병까지 연결된다. 신체적 노쇠를 보이는 경도 인지 장애 환자에서의 신경 활동 변화와 동적 뇌 네트워크 재구성 변화에 대한 연구는 아직까지 보고된 바가 없으며, 본 연구 결과를 통하여 뇌 영상 데이터가 인지 노쇠의 중요한 바이오마커의 역할을 할 것으로 기대된다.

본 연구에서는 [^{18}F]FDG PET 과 rs-fMRI 뇌 영상 검사를 총 48 명의 경도 인지 기능 장애 환자 (신체적 노쇠가 없는 대조군: 21 명, 평균 연령 = 74.7 ± 5.8 세; 신체적 노쇠가 있는 위험군: 27 명, 평균 연령 = 75.5 ± 7.3 세)를 대상으로 진행하였다. 본 연구의 첫번째 부분에서는 위험군에서의 뇌 영역의 포도당 대사의 변화와 regional homogeneity 를 이용한 뇌 활동 변화를 조사하였다. 위험군에서는 우측 전두피질, 전대상피질, 양측 상두정소엽에서 뇌 대사 감소가 나타났고, 상두정소엽에서의 대사 변화와 악력, 집행 기능과 양의 상관 관계를 보였다. 뇌 영역의 regional homogeneity 변화는 양측 꼬리핵, 우측 내측과 가측 전두피질, 우측 상측두피질, 소뇌에서 감소하는 것으로 보였고, 꼬리핵과 상측두피질에서의 regional homogeneity 감소는 악력, 보행 속도, 신체 활동 감소 수치와 높은 상관성을 보였다. 또한, 언어 및 시공간 기능의 인지 수행 능력과 높은 상관 관계를 보이는 것을 관찰하였다.

본 연구의 두번째 부분은 위험군에서의 뇌 네트워크의 동적 기능적 연결성과 특징 변화를 살펴보았다. 동적 기능적 연결 분석은 sliding-window 방법과 k-means clustering 방법을 사용하여 뇌 네트워크 연결 구성 상태 (State)를 추정하였다. 휴지기 상태의 영상 촬영 시간 동안 총 4 개의 기능적 연결성 패턴이 발견되었고, 가장 자주 발생하는 State 1 은 주로 뇌 네트워크 내부 연결성을 보이고, 네트워크 간의 연결성은 약한 것이 특징으로 나타났다. 그 다음으로 자주 나타난 State 2, 3, 4 는 네트워크 간의 양과 음의 연결성 모두 강하게 나타났다. State 의 전환 수, fractional windows, mean dwell time 과 같은 시간적 속성의 그룹 비교 결과는 유의한 수준에 도달하지 못했지만, 위험군에서 State1 의 재발현이 감소되고 State 2, State 3 의 발현 증가가 나타나는 것으로 확인되었다.

State 1 의 속성 (fractional windows, mean dwell time)이 악력 및 신체 활동량과 양의 상관 관계를 나타냈고, 반면에, 디폴트 모드 네트워크 기능 연결성 증가가 특징적이었던 State 2 의 발현 증가 및 dwell time 증가는 낮은 MMSE-K 점수 저하와 상관이 있는 것을 관찰하였다. 네트워크 변화는 노화현상에서 관측되는 네트워크 기능적 분리 (functional segregation)의 감소를 나타내는 것으로 생각되며, 신체적 기능 저하가 이러한 현상을 촉진하는 것으로 보여진다. 뿐만 아니라, 위험군에서 감각운동 네트워크와 인지 기능 네트워크 간의 기능적 연결성과 인지 조절 네트워크 내부 연결성 세기에도 변화가 나타나는 것을 발견하였다.

결론으로는, 뇌 영상 분석 결과에서 인지 노쇠 위험군 환자에서 전두엽, 측두엽 그리고 두정엽에서 기능적 활동 변화가 나타나는 것을 관찰하였고, 이는 신체적 노쇠가 존재할 경우 병리학적 과정이 가속화되는 것으로 추정된다. 뇌 네트워크의 동적 기능적 연결성 분석을 통해 악력 감소와 함께 네트워크 기능적 분리 감소 현상이 두드러지는 것을 확인하였으며, 따라서, 뇌 영상 데이터가 인지 노쇠의 생체 표지자 역할을 할 수 있는 것으로 기대된다.

주요어: 인지 노쇠, FDG PET, rs-fMRI, regional homogeneity, 동적 기능적 연결성

학번: 2014-30671